Comparison of thermal and chemical enhanced recovery of DNAPL in saturated porous media: 2D tank pumping experiments and two-phase flow modelling

Stefan Colombano, Hossein Davarzani, E.D. van Hullebusch, D. Huguenot, Dominique Guyonnet, Jacques Deparis, Fabien Lion, Ioannis Ignatiadis

Comparison of thermal and chemical enhanced recovery of DNAPL in saturated porous media: 2D tank pumping experiments and two-phase flow modelling

S. Colombano[1*], H. Davarzani[1], E.D van Hullebusch[2], D. Huguenot[3], D. Guyonnet[1], J. Deparis[1], F. Lion[1], I. Ignatiadis[1]

[1] BRGM (French Geological Survey), France

[2] Université de Paris, Institut de Physique du Globe de Paris, CNRS, F-75005 Paris, France

[3] Laboratoire Géomatériaux et Environnement, Université Gustave-Eiffel, France

*corresponding author: Email: s.colombano@brgm.fr. Phone: (33) (0)6 78 48 50 41

Abstract

Pumping experiments were performed in a 2D tank in order to estimate the recovery yield of pure heavy chlorinated organic compounds (DNAPL; dense non-aqueous phase liquids) by varying different parameters: permeability of the saturated zone, pumping flow rates, addition of surfactant and heating. Surfactant was added to decrease capillary forces involved in the entrapment of DNAPL in porous media while temperature was increased to reduce DNAPL viscosity (and hence increase its mobility). Chemical enhancement was performed with the addition of Sodium Dodecyl Benzene Sulfonate (SDBS) (at its Critical Micelle Concentration, to avoid DNAPL dissolution) and thermal enhancement was performed at 50 °C (to avoid DNAPL volatilization). The experiments were monitored with photography allowing, on the basis of image interpretation, to convert optical densities (OD) into water saturations (S_w). Image interpretations were compared with modelling results. The two-phase flow modelling was performed with the pressure-pressure formulation using capillary pressure and relative permeability functions based on the van Genuchten – Mualem equations. Measured volumes of DNAPL recovered as well as the displacement of the DNAPL-water interface (radius and height of the cone of depression) are consistent with the modelling results. Furthermore, chemical enhancement results in a significant increase in the recovery rates of DNAPL. The observed improvement in the recovery of DNAPL with chemical enhancement is due to the fact that: (i) the residual saturation inside the cone of depression is lower and (ii) the cone of depression radius and height increase. Thermal enhancement had no beneficial effect on DNAPL recovery rate or yield. This study shows that it is possible to accurately determine water and DNAPL saturations by image interpretation during pumping tests in a 2D tank in the laboratory. For field-scale applications, the two-phase flow model allows to determine remediation yields as well as the volumes of the cone of depression according to the different operating conditions.

Keywords

Dense Non-Aqueous Phase Liquids, chemical enhancement, thermal enhancement, free product recovery, two-phase flow modelling, optical density.

1. Introduction

Chlorinated Organic Compounds (COCs) have been produced in large quantities since the middle of the 20th century mostly as solvents, pesticides, electrical insulators [Cohen and Mercer (1993); Kueper et al. (2003)]. COCs are recognized as among the most health-threatening chemicals detected in groundwater [Mackay et al. (1985)]. These particularly toxic pollutants may permanently contaminate soil, indoor air, and groundwater [ADEME and Ernst & Young (2014); NIEHS (2015); IARC (2018)]. COCs are often very hydrophobic and are denser than water. In the event of pollution, COCs infiltrate into the vadose and saturated zones down to the substratum to form DNAPL (Dense Non-Aqueous Phase Liquid) pools [Schwille (1988); Cohen and Mercer (1993)]. The light COCs dissolve and volatilize and thus generate large contaminant plumes leading to severe groundwater contamination [Stupp and Paus (1999); Sale (2001); Stroo et al. (2003); Falta et al. (2005a); Falta et al. (2005b); McDade et al. (2005); Newell and Adamson (2005); McGuire et al. (2006); Huang et al. (2015)]. The recovery of DNAPL free-phase (mobile) product is therefore a priority in order to avoid its migration and its dissolution. This recovery is mainly performed using the pump and treat method. These methods are time-consuming (*e.g.,* commonly more than 30 years) and are not very efficient [Mackay and Cherry (1989); Travis and Doty (1990); Berglund and Cvetkovic (1995); Pankow and Cherry (1996); Falta et al. (2005b); McDade et al. (2005); McGuire et al. (2006); Harkness and Konzuk (2014)]. Typical recovery yields following pumping do not exceed 60% [ITRC (2002); Stroo et al. (2012)].

The DNAPL studied herein was sampled from the Tavaux site; a large chloralkali chemical plant located in the center-east of France. This DNAPL is a mixture of heavy chlorinated organic compounds (weight percent; wt%): hexachlorobutadiene-HCBD (58%), hexachloroethane-HCA (14%), perchloroethylene-PCE (8%), and pentachlorobenzene-PCB (3.5%), carbon tetrachloride-CT (4%), trichloroethylene-TCE (2%), hexachlorobenzene-HCBE (1%) [Cazaux et al. (2014)].

Surfactant addition aims to decrease the interfacial tension (IFT) between the organic phase and water and to increase NAPL solubility in water through micelle generation (once surfactant concentrations exceed the Critical Micelle Concentration; CMC) [Rosen (1989); Pennell et al. (2014)]. Several surfactants (*i.e.,* Triton X-100, Tween 80, Aerosol MA-80 and SDBS) are able to solubilize

and reduce the IFT for the TCE-water and PCE-water systems [Taylor et al. (2001); Zhong et al. (2003); Zhao et al. (2006); Suchomel et al. (2007); Harendra and Vipulanandan (2011); Atteia et al. (2013); Pennell et al. (2014)]. For TCE, the addition of Aerosol-MA-80 can reduce the IFT from 35.2 to 0.2 $mN.m^{-1}$ [Dwarakanath et al. (1999)], while adding Tween 80 decreases IFT from 35.2 to 10.4 $mN.m^{-1}$ [Suchomel et al. (2007)]. For PCE, the addition of different surfactants is also effective in reducing the IFT: Aerosol [Dwarakanath et al. (1999); Sabatini et al. (2000); Childs et al. (2004)], Triton X-100 and Tween 80 [Taylor et al. (2001); Harendra and Vipulanandan (2011)]. Pennell et al. (2014) listed 16 representative examples of surfactant flushing field demonstrations with chlorinated compounds (mainly PCE and TCE) and showed remediation yields varying between 68 and 98%. The DNAPL investigated in the present study does not contain more than 15% (wt%) of these compounds. No research work has yet been done on the IFT of the main compounds encountered in the Tavaux DNAPL (*i.e.,* HCBD and HCA). Colombano et al. (2020) have shown that the addition of SDBS at its CMC, decreased interfacial tensions of the Tavaux DNAPL by a factor of 12. In this work, SDBS was introduced at its CMC, in order to avoid DNAPL dissolution, which generates costly water treatment technologies [Sabatini et al. (1998); Ahn et al. (2008); Atteia et al. (2013); Maire et al. (2018)].

As the effect of temperature on NAPL behaviour in porous media is influenced by several parameters (relative permeability, interfacial tension, viscosity, density, and wettability, …), the effect of thermal enhancement on NAPL behaviour is difficult to predict [Esmaeili et al. (2019); Philippe et al. (2020)]. Davis (1997) showed that the viscosity of a chlorinated solvent is generally reduced by 1% per degree Celsius incremental increase [Davis (1997)]. Significant reductions in PCE viscosities with increasing temperatures have been reported [Sleep and Ma (1997)]. Various studies have shown that increasing temperatures tends to: decrease volumes of trapped non-wetting phase [Poston et al. (1970); Sinnokrot et al. (1971); Hopmans and Dane (1986); Grant and Salehzadeh (1996); Adamson and Gast (1997)], decrease entrapped air volumes [Hopmans and Dane (1986)], decrease residual PCE and increase irreducible water value [She and Sleep (1998)].

We used optical density to calibrate water saturation variations in a 2D tank. Two types of optical imaging methods are described in the literature: the Light Reflection Methods (LRM) and Light Transmission Methods (LTM) [Alazaiza et al. (2016)]. O'Carroll et al. (2004) used LRM to estimate

88 the saturation of PCE and reported a linear relationship between the colour variations and PCE
89 saturation (with a correlation R^2 value of 0.91) [O'Carroll et al. (2004)]. Luciano et al. (2010) also
90 obtained satisfactory results: the difference between weight scale and image interpretation with LRM
91 was 6% [Luciano et al. (2010)]. Colombano *et al.* (2020) performed optical calibration experiments
92 with Tavaux DNAPL using the LRM method. They showed that the Optical density (OD) varied
93 linearly as a function of water saturation (S_w), even in the presence of surfactants and with thermal
94 enhancement [Colombano et al. (2020)].
95 In order to better understand the governing phenomena, the DNAPL pumping process was
96 simulated with and without thermal and chemical enhancement. There are several formulations for
97 modelling two-phase flow in porous media: the phase pressure-saturation formulation, the pressure-
98 pressure formulation, the flooding formulation, the fractional flow formulation, and the two-phase
99 mixed formulation [Antontsev (1972); Chavent and Jaffre (1986); Wang and Beckermann (1993);
100 Chen and Ewing (1997); Bastian (1999); Chen et al. (2006); Bjørnarå and Aker (2008); Ataie-Ashtiani
101 and Raeesi-Ardekani (2010)]. These equations are used to predict water and DNAPL saturations as
102 well as the DNAPL-water interface displacement. To the best of the authors' knowledge, this is the
103 first study that compares and models, simultaneously, the thermal and chemical enhanced recovery of
104 a complex DNAPL collected from a real polluted site in a non-consolidated porous medium.
105 Here, the main goal is to determine how chemical enhancement and thermal enhancement affect
106 DNAPL recovery yields during pumping experiments. This work focuses on the mobilization of the
107 free product while avoiding solubilization and volatilization of COCs (in the aqueous and gas phases,
108 respectively). Therefore, we added SDBS at its CMC (to avoid DNAPL dissolution), while heating
109 was limited to 50 °C (to avoid DNAPL volatilization). While enhancement was studied by
110 [Colombano et al., 2020] in instrumented 1D cells, this paper addresses DNAPL pumping experiments
111 performed in a 2D tank to validate the two-phase flow model and to compare the modelled water
112 saturations with the data obtained from the imaging data processing. The experiments were performed
113 with a DNAPL mixture collected in the field and a porous media made of glass beads (GB). The use of
114 glass beads helped avoid potential artefact effects associated with porous medium heterogeneity.

Several operational conditions were changed during these experiments: permeability of the saturated zone, pumping flow rates, the addition of surfactant and heating.

2. Materials and methods

The DNAPL pumping experiments in the 2D tank were performed with two types of glass beads, at different flow rates, without enhancement at 20 °C, with chemical enhancement (with SDBS-sodium dodecyl benzene sulfonate) at its CMC (to avoid DNAPL dissolution) and/or thermal enhancement at 50 °C (to avoid DNAPL volatilization). SDBS was supplied by Sigma Aldrich (laboratory grade). The DNAPL used for the experiments was sampled at the Tavaux site and stored at 4 °C until use. DNAPL was filtered to eliminate the potential dust just before its use (EMD Millipore, 0.45 µm). The water used for all experiments was local tap water degassed using VWR Ultrasonic Cleaner (USC500D: 60 °C,
45 Hz, 60 min). The physical parameters of the DNAPL and water, with and without enhancement, are presented in Table 1.

Table 1: Physical parameters of the DNAPL and water with and without enhancement [Colombano et al. (2020)].

Parameters	Density ($kg.L^{-1}$)	Dynamic viscosity (mPa.s)	DNAPL/water interfacial tension ($mN.m^{-1}$)	DNAPL/water/glass contact angle (°)
DNAPL, 20 °C, without SDBS	1.661±0.005	4.473±0.150	10.96±0.05	119.33±4.16
DNAPL, 20 °C, with SDBS	1.661±0.005	4.473±0.150	1.05±0.11	92.33±2.52
DNAPL, 50 °C, without SDBS	1.634±0.002	2.832±0.06	11.90±0.10	107.67±2.52
Water, 20 °C	0.998±0.002	1.002±0.003	-	-
Water, 50 °C	0.988±0.002	0.546±0.002	-	-

2.1 *DNAPL pumping experiments in the 2D tank*

The dimensions of the 2D tank, made of polyvinylidene difluoride (PVDF), were: length = 50 cm, height = 30 cm and width = 7 cm. The front portion of the 2D tank was made of glass to allow photography of the two-phase flow process. The main tank is composed of a central reservoir for the porous medium and two counter-channels (cavities) on both sides for static level regulation (Figure 1 and Figure 2). Counter-channels are connected with the central reservoir through a metallic grid that lets fluids pass through but constrains the glass beads inside the central reservoir. The 2D tank is thermo-regulated using internal double-wall ducts inside and between the two glasses. A "LAUDA" water bath (model ECO RE 420) was used for circulating water inside this double-wall duct. It was filled with a thermo-regulated water bath via a closed system which makes the water circulate from the water bath to the internal tank, from the internal tank to the double-glazing, and finally back to the water bath.

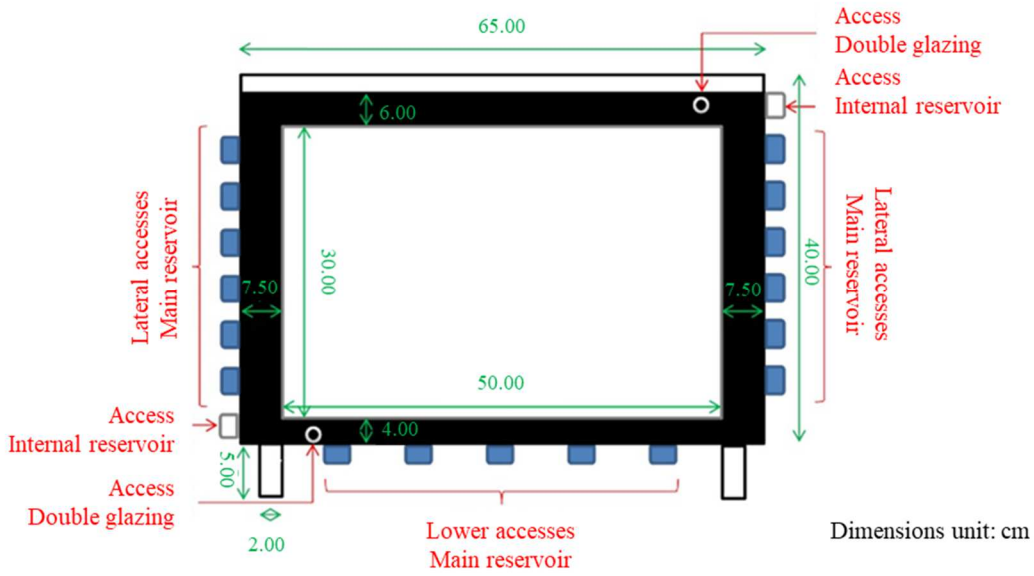

Figure 1: Schematic of the experimental 2D tank, its main features, and dimensions.

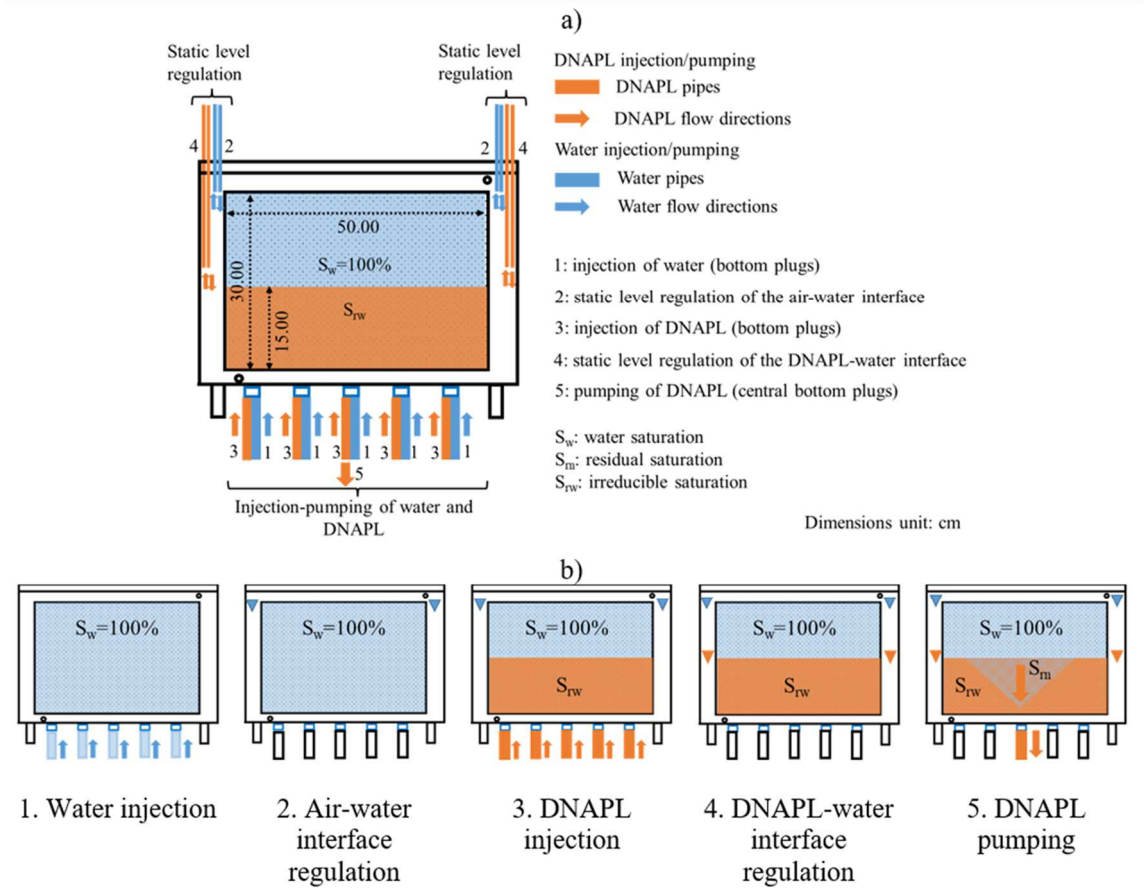

Figure 2: Principle of the injection and pumping device for water and DNAPL: a) schematic of the experimental 2D tanks and b) detailed experimental protocol step with: 1) water injection, 2) air-water interface regulation, 3) DNAPL injection, 4) DNAPL-water interface regulation, 5) DNAPL pumping.

The 2D tank was filled with GB (30.0 cm of height). Two sizes of GB, supplied by Next Advance, were used: 0.10 ± 0.02 mm ($k = 6.73\times10^{-12}$ m^2) and 0.5 ± 0.1 mm GB ($k = 1.30\times10^{-10}$ m^2). The 2D tank was connected to peristaltic pumps to inject and pump water as well as DNAPL. The liquids were pumped from or injected into graduated cylinders to measure the liquid volumes. The mass of DNAPL was also monitored using a weight scale (Sartorius Cubis MSE8201S-000-D0) with an automatic data acquisition. Two types of peristaltic pumps were used: Watson Marlow 205 and Watson Marlow 530U. The five bottom lines were used to initially saturate the porous medium (at a flow rate of 0.05 mL.min^{-1}) with water from the bottom (step 1: pipes and arrows at the bottom in blue in Figure 2) until reaching a height of 30.00 cm. Four pumping and injection pipes, inserted inside each counter-channel, were used to regulate the level of the air-water interface at a height of 30.00 cm (step 2: pipes

and arrow in blue in the counter-channels in Figure 2). Then we injected the DNAPL (from the bottom) to a height of 15.00 cm (to reach the irreducible saturation, S_{rw}) at a flow rate of 0.01 mL.min^{-1} (step 3: pipes and arrows at the bottom in brown in Figure 2). S_{rw} were 0.24 and 0.30 for 0.5 and 0.1 mm GB, respectively. Four additional pumping and injection pipes, inserted inside each counter-channel, were used to regulate the level of the DNAPL-water interface at a height of 15.00 cm (step 4: pipes and arrows in brown in the counter-channels in Figure 2). Then, the central bottom line was used to pump out the DNAPL (step 5: pipe and arrows in brown in Figure 2). The experiments were carried out at different DNAPL pumping flow rates (50, 150, 220 mL.min^{-1}). The pumping and injection flow rates of DNAPL and water used to regulate these two levels were adapted to the pumping flow rates of DNAPL from the central bottom line. Photographs were taken during the pumping experiments to quantify the evolution of DNAPL saturation in the 2D tank as a function of time.

2.2 Image interpretation

The purpose of image analysis was to capture changes in the two-phase flow over time inside the porous medium and to estimate DNAPL saturation. The digital camera used in this study was a Nikon® D810 with NIKKOR LENS 105 (Nikon®). The experiments were performed in a dark room and the light source was provided by two 300 W floodlights (Broncolor®). To avoid any reflections and to optimize the contrast that is required for the interpretation, black and white reflectors were set up at precise locations in the laboratory. A greyscale was placed beside the 2D tank to calibrate the differences, albeit small, between the lighting used for the various experiments. The image interpretation process was performed as follows (Figure 3).

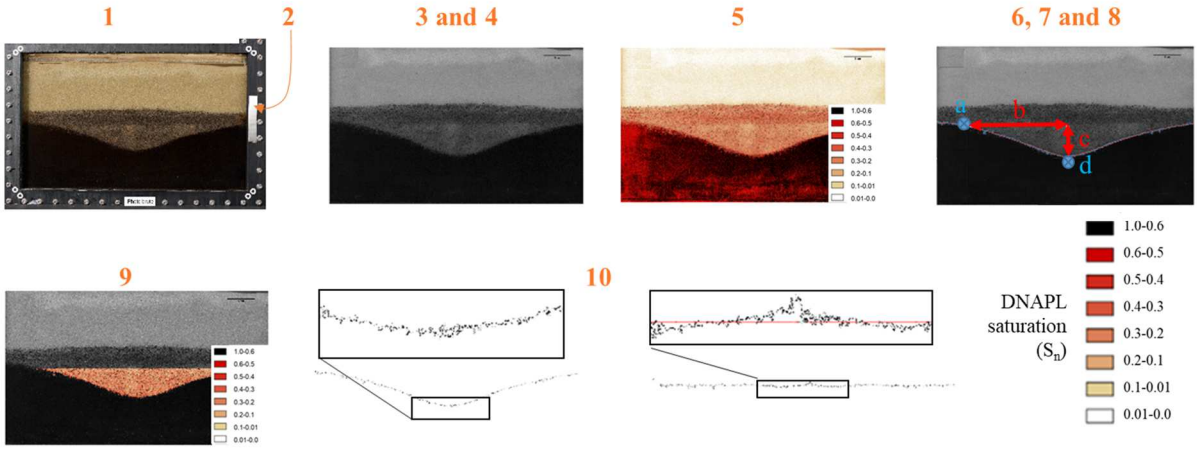

Figure 3: Image interpretation procedures: 1) Acquisition of the raw Nikon photographs, 2) Light intensities rectification using the target, 3) Conversion of the image into B&W 8-bit format to obtain 256 shades of grey, 4) Scaling and orthogonalization of the images, 5) Estimation of total residual saturations (whole Area Of Interest-AOI), 6) Automatic detection of the DNAPL-water interface by contrast optical intensity, 7) Estimation of the shape of the cone of depression, 8) Measurement of the height and radius of the cone of depression (using the equation of the cone of depression obtained from point 6), 9) Estimation of the residual saturations inside the cone of depression, and 10) Estimation of fingering effects (from the interface detected in point 5). In steps 6 to 8: a) point of inflexion of the cone of depression, b) radius of the cone of depression, c) height of the cone of depression, and d) lower point of the cone of depression.

These image processing steps, based on the greyscale, imply that the converted images have the same characteristics in terms of dimensions (number of pixels) and luminosity. First of all, the photographs (126 pixels.cm^{-1}, *i.e.* 0.006 mm².pixel^{-1}) are converted into Black & White (B&W) 8-bit format to obtain 256 shades of grey according to the procedure described. Then, we checked whether the images had the same light intensities and contrasts at each location in the photograph, using the greyscale. The area of interest (AOI, length = 47.00 cm, height = 27.50 cm) for image interpretation was slightly smaller than the 2D tank glass surface to exclude the wall shade effect on the water saturation calculation.

206 The optical density of reflected light, D_r, can be defined as (Eq. 1 and Eq. 2) [Stimson (1974);
207 Schincariol et al. (1993); Flores et al. (2011)]:

$$D_r = -\log(\rho_t) \quad \text{Eq. 1}$$

$$\rho_t = \frac{I_r}{I_0} \quad \text{Eq. 2}$$

208 where: D_r = OD (-) is the optical density of reflected light, ρ_t (-) is the ratio of reflected/initial
209 luminous intensity, I_r (-) is the reflected luminous intensity and I_0 (-) is the initial luminous intensity.
210 The relationship between the optical density and the DNAPL saturation was determined as follows
211 [Colombano et al. (2020)]. Drainage and imbibition experiments were performed in a small 2D cell
212 (length = 5.00 cm, height = 5.00 cm, and width = 2.00 cm) using the same couples of fluids and the
213 same GB. The average optical density in the small 2D cell was determined for S_w=100%, S_w=0%, S_{rn}
214 and S_{rw}. A linear relationship was found between the optical density and DNAPL saturation:
215 D_r = -1.4477S_w + 1.7599.
216 Total DNAPL Saturation (S_n) was then determined in the AOI of the 2D tank, using two methods
217 based on optical densities: a "counting box" and a "layers" method [O'Carroll et al. (2004); Luciano
218 et al. (2010); Alazaiza et al. (2016)].
219 The counting box method consists in determining the average optical density in a square of pixels
220 (here 50×50 pixels) and then to consider the sum of these average optical densities calculated for the
221 whole AOI. The square size was selected to ensure the best compromise between measurement
222 accuracy and calculation time. By adding these averages, we determined the volume of DNAPL using
223 Eq. 4:

$$V_{DNAPL} = S_{DNAPL} A_{DNAPL} w \emptyset \quad \text{Eq. 3}$$

224 where V_{DNAPL}(m^3) is the volume of DNAPL for a given saturation, S_{DNAPL} (-) is the DNAPL
225 saturation calculated using Fiji software, A_{DNAPL} (m^2) is the saturation calculation area, w (m) is the
226 2D tank internal width, and Ø (-) is the porosity.
227 The layers method consists in determining which areas in the AOI have optical densities within a
228 determined interval. This interval is called a "layer". By adding the DNAPL saturation values that
229 come from different layers, we determined the volume of DNAPL using Eq. 3. Preliminary results

showed that the layers method provided more accurate estimates of pumped DNAPL volume variations than the counting box method. This is related to the fact that during pumping, the squares along the DNAPL-water interface correspond in part to S_{rn} and to S_{rw}. Therefore, we used only the layers method to calculate DNAPL saturation.

The interface was detected based on the difference in shades of grey between S_{rw} and S_{rn} (irreducible and residual saturation, respectively). The interface was manually fixed by iteration using expert judgment to best fit the cone of depression visible on the photograph. This operation used Fiji (an open-source platform for biological-image analysis). The interface obtained is made up of a multitude of points whose coordinates were extracted in Excel. The shape of the cone of depression can be estimated using the Hill's slope from a Four-Parameter Logistic Regression (Eq. 4).

$$y = d\frac{a - d}{1 + \left(\frac{x}{c}\right)^b} \qquad \text{Eq. 4}$$

where a (-) and d (-) are, respectively, the minimum and maximum values that can be obtained, c (-) is the point of inflection, and b (-) is the Hill's slope of the curve.

The height and radius of the cone of depression in each photograph were automatically calculated from Eq. 4 (using an Excel macro to fit the equation to the cone of depression). The areas of the cone of depression were also determined in each photograph. Next, averaged S_n was calculated over the cones of depression surfaces. This approach was selected because it was sometimes difficult to maintain the pressure heads on the edges of the 2D tank. The variation of the DNAPL-water interface led to a displacement of the DNAPL-water interface (upwards or downwards) and therefore to a change of the global S_n (S_n in the AOI).

Next, fingerings were estimated to characterize more precisely the DNAPL-water interface displacements. To achieve this, the shape of the cone of depression was estimated based on Eq. 4; and was compared to the actual interface between the DNAPL and water. The estimated interface and the actual interface were then flattened using Fiji (transposing the fitting curve into a horizontal axis, y). This flattening is necessary for the statistical study of the fluctuation height interface. Statistical comparison using XLSTAT then showed the differences between the estimated and measured DNAPL-water interface (standard deviation, percentile, etc.).

256 The tasks were automated using several scripts programmed in VBA for Excel and with ImageJ
257 Macro [Schindelin et al. (2012); Rueden et al. (2017)]. Other specific plugins used were: Find eyelets
258 [Tseng (2011)], Find the blank on the greyscale [Herbert et al. (2014)], Orthogonalization [Schlüter
259 (2008)].
260
261 **3. Theory**
262 *3.1 Governing Equations*
263 The local-scale governing equations for multiphase flow in porous media can be derived by
264 considering the averaging over the pore scale. By assuming that fluids and porous media are
265 incompressible, flow is laminar, DNAPL is non-soluble, and disregarding any reactions, mass balance
266 equations for wetting (subscript "w") and non-wetting (subscript "n") phases can be written as (Eq. 5
267 and Eq. 6) [Bear (1972)]:

$$\emptyset \frac{\partial(\rho_w S_w)}{\partial t} - \boldsymbol{\nabla}.\left[\rho_w \frac{\mathbf{k_{ij}}\, k_{r,w}}{\mu_w}(\boldsymbol{\nabla} P_w - \rho_w \mathbf{g}\boldsymbol{\nabla} z)\right] = 0 \qquad \text{Eq. 5}$$

$$\emptyset \frac{\partial(\rho_n S_n)}{\partial t} - \boldsymbol{\nabla}.\left[\rho_n \frac{\mathbf{k_{ij}}\, k_{r,n}}{\mu_n}(\boldsymbol{\nabla} P_n - \rho_n \mathbf{g}\boldsymbol{\nabla} z)\right] = 0 \qquad \text{Eq. 6}$$

268 where Ø (-) is the porosity, S (-) is the saturation of the fluid, $\mathbf{k_{ij}}$ (m^2) is the tensor of intrinsic
269 permeability, k_r (-) is the relative permeability, μ (Pa.s) is the dynamic viscosity, P (Pa) is the pressure,
270 g ($m.s^{-2}$) is the gravitational acceleration, z (-) is the direction of gravity.
271 Phase pressures are linked through the capillary pressure as follows (Eq. 7):

$$P_c(S_w) = P_n - P_w \qquad \text{Eq. 7}$$

272 where P_c (Pa) is the capillary pressure.
273 The sum of the phase saturations is equal to one (Eq. 8):

$$S_w + S_n = 1 \qquad \text{Eq. 8}$$

274 We used pressure-pressure formulations to solve the above-mentioned equations [Chen et al.
275 (2006); Ataie-Ashtiani and Raeesi-Ardekani (2010); Davarzani et al. (2014)].
276 The capillary pressure function and relative permeability function used were based on the van
277 Genuchten-Mualem (VGM) equations (Eq. 9 to Eq. 13) [Mualem (1976); van Genuchten (1980)].

$$S_{ew} = \frac{1}{[1 + (\alpha h_c)^n]^m} \quad \text{Eq. 9}$$

$$m = 1 - \frac{1}{n} \quad \text{Eq. 10}$$

$$S_{ew} = \frac{S_w - S_{rw}}{1 - S_{rw} - S_{rn}} \quad \text{Eq. 11}$$

$$k_{rw} = S_{ew}^{0.5}\left[1 - \left(1 - S_{ew}^{\frac{1}{m}}\right)^m\right]^2 \quad \text{Eq. 12}$$

$$k_{rn} = (1 - S_{ew})^{0.5}\left(1 - S_{ew}^{\frac{1}{m}}\right)^{2m} \quad \text{Eq. 13}$$

where S_{ew} (-) is the effective saturation of water saturation, h_c (m) is the capillary pressure head, α (m^{-1}) is the fitting parameter inversely proportional to the non-wetting fluid entry pressure value, n (-) is the width of pore-size distribution and S_r (-) is the residual saturation.

Releasing a source of DNAPL pure product (mass flow in dissolved phase) depends not only on groundwater characteristics and the primary physical and chemical characteristics of DNAPL but also on the characteristics of each source: i) magnitudes (particularly in the DNAPL/water interface); ii) ganglia-to-pool mass (GTP) ratio; iii) how the pores are connected (permeability); iv) morphometric properties of the sources; and v) residual saturations [Miller et al. (1990); Imhoff et al. (1993); Nambi and Powers (2003); Falta et al. (2005b); Falta et al. (2005a); Grant and Gerhard (2007a); Grant and Gerhard (2007b); Carey and McBean (2010a); Carey and McBean (2010b); Alexandra et al. (2012); Luciano et al. (2012); Luciano et al. (2018)].

In our study, the DNAPL bulk is composed mainly of very heavy and very poorly soluble COCs (HCBD, HCA, PCB: 75% (w/w)) but also of more conventional COCs (TCE, PCE). The sum of the COCs quantified and solubilized from DNAPL was: 44.0±5.2 $mg.L^{-1}$ (at 20°C), 47.5±2.5 $mg.L^{-1}$ (with SDBS at the CMC), 58.00±2.89 $mg.L^{-1}$ (at 50°C) [Colombano et al. (2020)]. The solubility of these heavy COCs is much lower than conventional COCs (for example the solubilities of TCE and PCE are 1100 and 160 $mg.L^{-1}$, respectively) [Rodrigues et al. (2017)]. Co-solubility explains the low solubility of the DNAPL bulk [Fredenslund et al. (1975); Banerjee (1984); Feenstra et al. (1991); Mackay et al. (1991)]. The DNAPL dissolved phase represents less than 0.1% (w/w) of the total mass of DNAPL in

297 the 2D tank. Moreover, during the experiments, almost 100% of the liquid recovered was DNAPL (the
298 bottom of the cone of depression did not reach point 6 - see Figure 4). Thus, the dissolution of
299 DNAPL was not considered in the model.
300
301 *3.2 Construction of the model, initial values, and boundary conditions*
302 The system of partial differential equations in a two-dimensional domain was solved using the
303 COMSOL Multiphysics® software, a commercial finite element software package.
304 The dimensions were chosen to be the same as the experimental setup ones. Two subdomains were
305 built: an upper subdomain (subdomain 1), which is only concerned with single water phase flow,
306 neglecting the capillary effect at its interface, and a lower subdomain (subdomain 2), which is
307 concerned with the two-phase flow of water and DNAPL. According to the experimental procedures,
308 the initial conditions were the hydrostatic pressures with $P_w=\rho_w g(0.3-y)$ and $P_n=P_0+\rho_n g(0.15-y)$, where
309 P_0 is the pressure needed to obtain a known initial saturation (here S_{rw}) and y is the height. Values
310 were 2300 Pa and 1700 Pa for 0.1 mm GB and 0.5 mm GB, respectively. Figure 4 shows the boundary
311 conditions for imbibition in the 2D tank experiments.
312

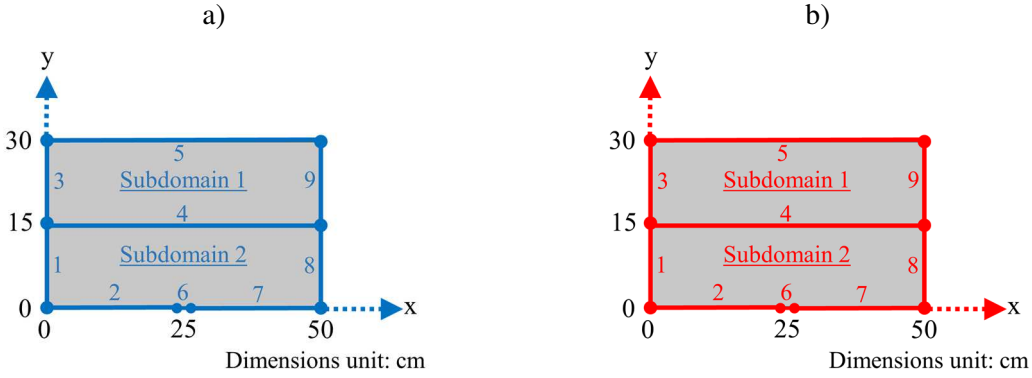

2, 6, 7: no flow
4: not applicable
1, 3, 5, 8 and 9: $P_w=\rho_w g(0.3-y)$

2, 4, 7: no flow
1 and 8: $P_n=P_0+\rho_n g(0.15-y)$
6: pumping flow rate of the DNAPL

313 Figure 4: Boundary conditions for primary variables a) P_w and b) P_n.
314
315 The pumping experiments were performed at irreducible saturation (S_{rw}). At this saturation, the
316 DNAPL phase is mobile because of the continuum, while the water phase is immobile (discontinued

317 phase). At S_{rw}, the relative permeabilities of the wetting and non-wetting phases are (Eq. 12 and Eq. 13):
318 for 0.5 mm GB: k_{rn}=0.54 and k_{rw}=0.02, and for 0.1 mm GB: k_{rn}=0.43 and k_{rw}=0.02. Thus, we have set
319 the boundary condition in point 6 (bottom) as follows: pumping flow rate for DNAPL and no flow for
320 the water phase. Monitoring the quantities of DNAPL recovered shows that this hypothesis is correct
321 as long as the bottom of the cone of depression does not reach point 6. The experiments were
322 interupted when the steady-state was reached (for the case where the bottom of the cone of depression
323 did not reach point 6) or before the bottom of the cone of depression reached this point. In other
324 configurations, it was necessary to introduce a water flux.

325 The capillary pressure-water saturation relationship under different conditions (thermal and
326 chemical enhancement) and for the GB 0.1 mm and 0.5 mm were measured using an instrumented
327 small 1D cell (see [Colombano et al. (2020)] for a detailed description of the experimental
328 procedures). The experimental data were fitted to the VGM function to obtain the necessary input
329 parameters for the two-phase flow model. The VGM parameters and residual saturations are listed in
330 Table 2 (partially from [Colombano et al. (2020)]).

331

332 Table 2: VGM parameters and irreducible and residual saturations for 0.5 and 0.1 mm GB with and
333 without enhancements (partially from [Colombano et al. (2020)]).

Parame-ters	0.5 mm GB - Imbibition			0.1 mm GB - Imbibition		
	Without enhancement	Chemical enhancement	Thermal enhancement	Without enhancement	Chemical enhancement	Thermal enhancement
α (m^{-1})	38.36	39.69	38.31	23.29	22.08	26.97
n (-)	5.15	4.37	4.84	16.98	4.98	4.16
SSE	0.0025	0.0018	0.0047	0.0214	0.00587	0.00393
S_{rn} (-)	0.109	0.079	0.101	0.127	0.068	0.123
S_{rw} (-)	0.248	0.243	0.225	0.309	0.315	0.305

334

335 The remediation enhancement yields obtained in the 1D cell experiments [Colombano et al. (2020)]
336 with SDBS (at its CMC) were 27.6% (*i.e.* S_{rn} = 0.079) for 0.5 mm GB and 46.3% (*i.e.* S_{rn} = 0.068) for
337 0.1 mm GB. The remediation enhancement yields for 0.1 mm GB were higher than those observed
338 with the 0.5 mm GB. This difference is due to the capillary forces, which were higher for 0.1 mm GB
339 (the effect of the surfactants, whose purpose is to reduce the IFT, is improved). No significant

340 improvement in the remediation yield was observed at 50 °C (S_{rn} values were very close with and
341 without thermal enhancement). Variations in the values of dynamic viscosity and density of DNAPL
342 and water as a function of temperature were also incorporated into the model [Colombano et al.
343 (2020)]. The modelling results were compared to the 2D tank experiments with and without
344 chemical/thermal enhancements. A sensitivity analysis of the model is presented in Figure 1A
345 (Appendix).
346
347 **4. Results and discussion**
348 *4.1 Experiments in the 2D tank without enhancement*
349 Several imbibition experiments were performed with the 2D tank: 3 experiments with 0.5 mm GB
350 and 3 experiments with 0.1 mm GB, for three different pumping flow rates (50, 150, and 220 mL.min^{-1}).
351
352 a) Comparison of the recovered DNAPL volumes estimated by weight scale and by image
353 interpretation
354 The recovered DNAPL volumes were measured by weight scale and volume measurements. These
355 masses converted into volumes (by considering the DNAPL density) were compared with the
356 recovered DNAPL volumes estimated by optical density monitoring (Figure 5).

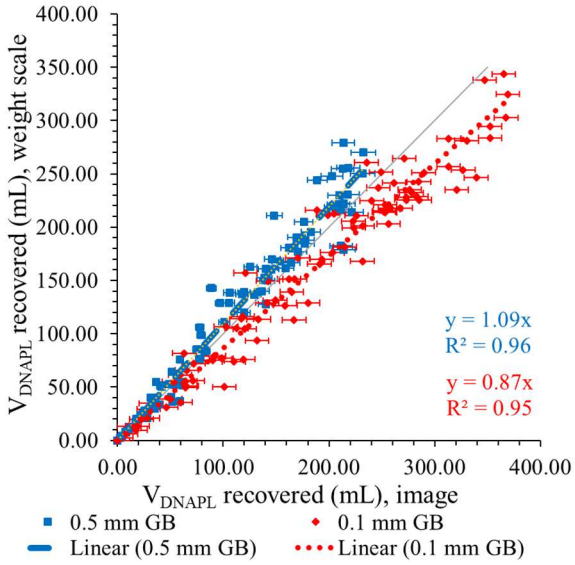

357

358 Figure 5: Comparison of the volumes of recovered DNAPL estimated using weight scale and with
359 image interpretation in the 2D tank with 0.5 and 0.1 mm GB (without enhancement) for 150 mL.min^{-1}.

The slopes of $V_{DNAPL\ recovered\ weight\ scale} = f(V_{DNAPL\ recovered\ image})$ were 1.09 and 0.87 respectively for 0.5 and 0.1 mm GB (R^2 of 0.96 and 0.95). These data show that the image interpretation allows a good overall estimation of the DNAPL saturations and the DNAPL volumes recovered.

b) Comparison of the recovered DNAPL volumes estimated by image interpretation and modelling

We compared modelling results with results from optical density monitoring, in terms of DNAPL volumes recovered and of DNAPL-water interface displacement (radius and height). Figure 6 shows the evolution of measured and modelled volumes of DNAPL recovered after pumping, for different pumping flow rates.

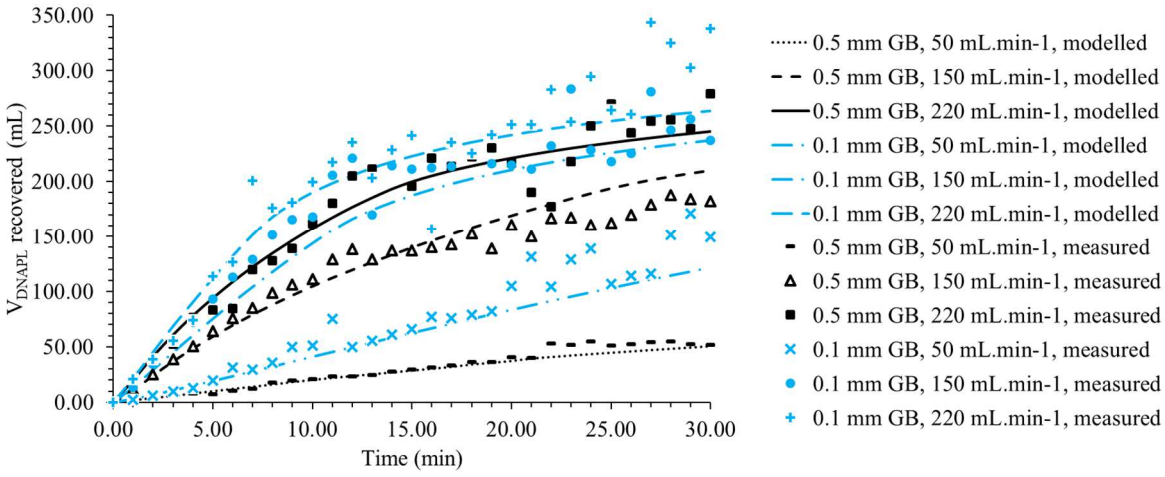

Figure 6: Evolution of measured (by image interpretation) and modelled volumes of DNAPL recovered for different flow rates with 0.5 and 0.1 mm GB (without enhancement).

Model results are consistent with experimental data. A more detailed description of the experiment/model comparison is presented below (see Figure 7 to Figure 9). The higher the flow rates, the more important was the recovered volume of DNAPL (V_{DNAPL}). For the same flow rates, V_{DNAPL} recovered were higher for 0.1 mm GB than for 0.5 mm GB. For low flow rates (50 $mL.min^{-1}$), the difference of V_{DNAPL} recovered between 0.1 and 0.5 mm GB increased over time. At the end of

pumping (t=30 min), V_{DNAPL} recovered were 51 mL and 149 mL for 0.5 and 0.1 mm GB, respectively. For higher flow rates (220 mL.min^{-1}), this difference of V_{DNAPL} recovered between 0.1 and 0.5 mm GB was lower (10 to 15%) and remained stable over time. For the flow rate of 150 mL.min^{-1}, this difference decreased at the end of the pumping (25% and 11% at t = 15 min and at t=30 min, respectively). The flow rate of DNAPL recovered decreased with time during the experiment (except for 50 mL.min^{-1}). The ratios of V_{DNAPL} recovered/flow rate for 50, 150, and 220 mL.min^{-1} were on average 0.034, 0.047, 0.037 (for 0.5 mmm GB) and 0.081, 0.053, 0.040 (for 0.1 mmm GB), respectively. Given the experimental conditions (the static DNAPL-water interface in the counter-channels of the 2D tank and the static air-water interface over the entire length of the 2D tank), these ratios were more important for 50 mL.min^{-1} (for 0.1 mm GB) and for 150 mL.min^{-1} (for 0.5 mm GB). These ratios decreased sharply during the experiment except for 50 mL.min^{-1}. These results confirm that from an application point of view, in such a high permeable porous media, it is beneficial to pump at lower flow rates in order to recover more DNAPL.

The measured and modelled surface DNAPL saturation during experiments as well as the measured and modelled DNAPL-water interface displacements (height, radius, and volume of the cone of depression – see Figure 3) were compared at different steps during the pumping experiments, for different pumping flow rates and GB sizes (Figure 7 and Figure 8).

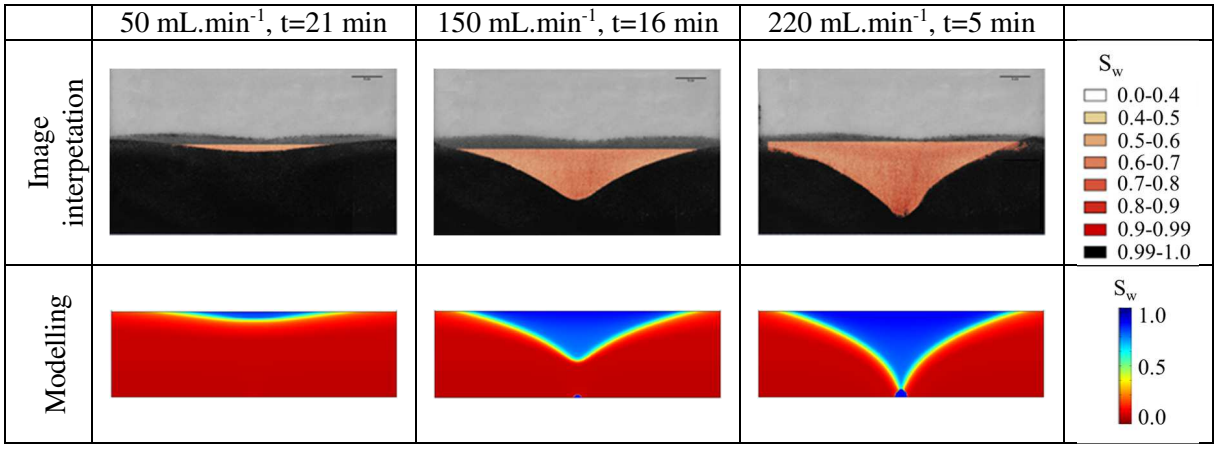

Figure 7: Comparison of measured (with image interpretation) and modelled cone of depression (0.5 mm GB) at the end of the pumping (steady-state condition).

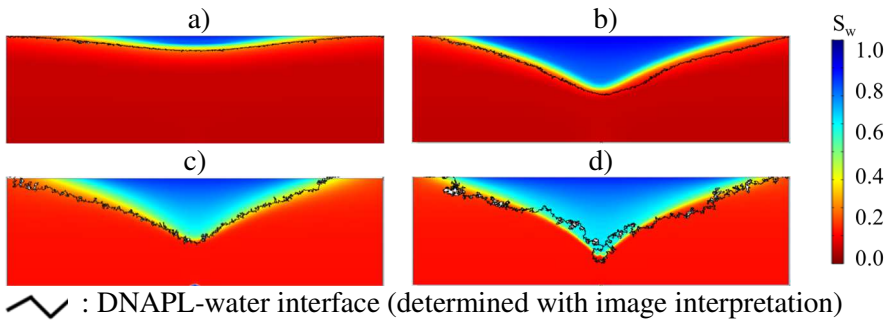

Figure 8: Comparison of measured and modelled DNAPL-water interface in the 2D tank at different times (without enhancement): a) 0.5 mm GB, 50 mL.min^{-1}, t=21 min; b) 0.5 mm GB, 150 mL.min^{-1}, t=16 min; c) 0.1 mm GB, 50 mL.min^{-1}, t=20 min; d) 0.1 mm GB, 220 mL.min^{-1}, t=5 min.

For 0.5 mm GB, at same flow rate, the depression surface area was lower than for 0.1 mm GB. This is due to the higher permeability, which generates a steeper DNAPL-water interface for 0.5 mm GB. Figure 7 and Figure 8 show how the modelled DNAPL-water interface displacement can be superimposed correctly with the experimental data obtained from image interpretation. As expected, the capillary fringe height modelled was greater for the 0.1 mm GB than for the 0.5 mm GB. Figure 2A (Appendix) shows how S_w changed as a function of time along the horizontal and vertical profiles located at the center of the tank. For the same flow rates, the cone of depression was higher for the 0.1 mm GB than for the 0.5 mm GB. In addition, the experimental results showed that the interface is much more tortuous for the 0.1 mm GB than for the 0.5 mm GB. This is due to the fact that the capillary effects are more important for 0.1 mm GB than 0.5 mm GB porous media (capillary fingering). Figure 9 shows the measured and modelled volumes of DNAPL recovered during experiments as well as the measured and modelled height and radius of the cone of depression (COD).

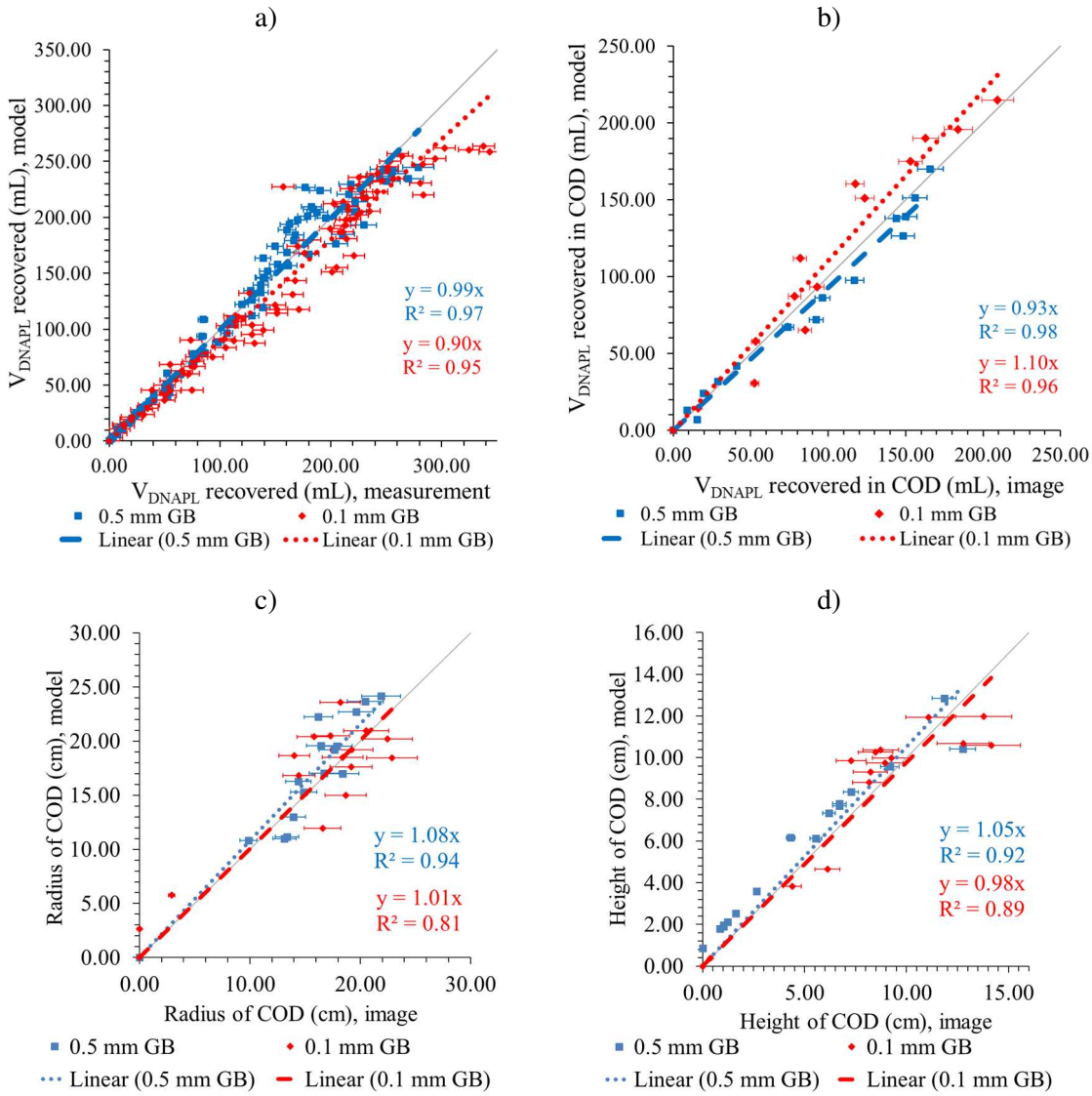

Figure 9: Comparison of experimental and modelled results in the 2D tank with 0.5 and 0.1 mm GB (without enhancement) for 150 mL.min^{-1}: a) volumes of recovered DNAPL estimated with image interpretation vs modelled volumes of DNAPL recovered, b) volumes of DNAPL recovered estimated with image interpretation vs modelled volumes of DNAPL estimated using the cone of depression zone, c) radius of the cone of depression estimated with image interpretation versus calculated with the model, and d) height of the cone of depression estimated with image interpretation versus calculated with the model.

One can see that the experimental and modelled volumes of DNAPL recovered were very similar (Figure 9a). The volumes of DNAPL were estimated with image interpretation over the AOI (see

Figure 3, point 5). The $V_{DNAPL\ measured}/V_{DNAPL\ modelled}$ ratios vary between 0.75 and 1.3 for 0.5 mm GB and between 0.69 and 1.65 for 0.1 mm GB. The linear regression curve gradients are very close to 1: 0.99 for 0.5 mm GB and 0.90 for 0.1 mm GB. The coefficients of determination were closer to 1 for the

0.5 mm GB (R^2=0.97) than for 0.1 mm GB (R^2=0.95), indicating as expected more data dispersion for the 0.1 mm GB than for 0.5 mm GB.

Figure 9b compares $V_{DNAPL\ recovered}$ estimated with image interpretation in the COD (see Figure 3, point 9) and modelled $V_{DNAPL\ recovered}$ in the COD (the volume of DNAPL related to lateral inflows are deduced from the total volume calculation). The slopes were close to 1 (0.93 for the 0.5 mm GB and 1.10 for the 0.1 mm GB). The R^2 coefficients are also close to 1 (respectively 0.98 and 0.96 for the 0.5 and 0.1 mm GB). Therefore, we conclude that the model can adequately reproduce the pumping process in 2D tank. The DNAPL recovered in the COD was about 209.46 and 166.17 mL for 0.5 and 0.1 mm GB, respectively. The average S_{rn} was about 0.11 for 0.5 mm GB and 0.13 for 0.1 mm GB, which corresponds to the values reported in the literature concerning chlorinated compounds. The S_{rn} for PCE is 0.15 to 0.2 for fine to medium sand and 0.08 for loamy sand and the S_{rn} for TCE vary between 0.002 and 0.2 for fine to medium sand [Lin et al. (1982); Cary et al. (1989); Poulsen and Kueper (1992); Cohen and Mercer (1993); ITRC (2015)]. These results are also consistent with the S_{rn} obtained during drainage-imbibition experiments in a 1D cells setup [Colombano et al. (2020)].

By comparing the radii and cone of depression heights, we can better assess how the model fits the experimental results (Figure 9b and c). The proposed model satisfactorily reproduces the shape of the cone of depression. The modelled and measured radii, the linear regression curve gradients were 1.08 (R^2= 0.94) and 1.01 (R^2=0.81) respectively for the 0.5 mm and 0.1 mm GB. For the cone of depression heights, linear regressions confirm the goodness of fit: the curves were respectively 1.05 (R^2=0.92) and 0.98 (R^2=0.89). The modelling of the experimental data was less accurate for the 0.1 mm GB than for the 0.5 mm GB. This can be explained by the fact that the fingerings and preferential pathways were more important for the 0.1 mm GB, which affects the experimental repeatability.

459 *4.2 Experiments in the 2D tank with chemical enhancement*

460 Figure 10 shows measured and modelled volumes of DNAPL as a function of time (without
461 enhancement as a reference case and with chemical enhancement).

462

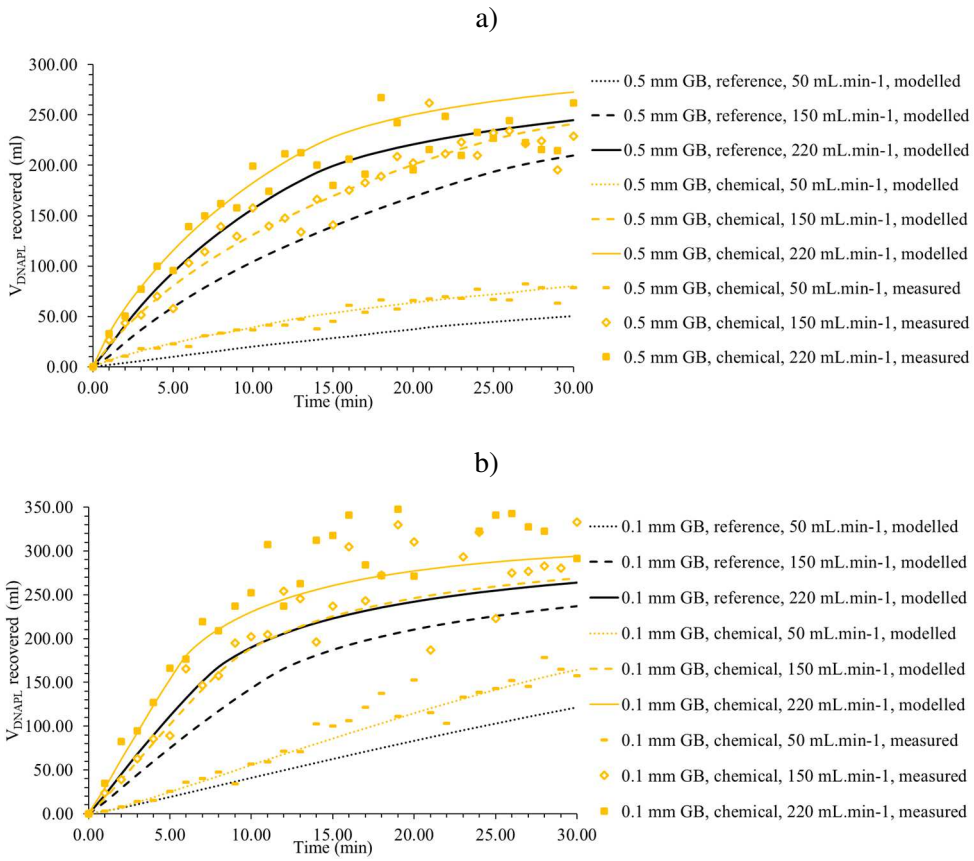

463 Figure 10: Evolution of measured (by image interpretation) and modelled volumes of DNAPL
464 recovered for different flow rates with a) 0.5 mm GB and b) 0.1 mm GB (with chemical
465 enhancement).

466

467 As previously stated, experimental and modelling results are consistent (see Figure 3A (Appendix)
468 for additional comparisons of experimental and modelling results). The chemical enhancement
469 increases the DNAPL recovered with the same flow rates when compared to the test performed
470 without enhancement. Figure 11 shows modelled $V_{DNAPL,\ chemical}/V_{DNAPL,\ reference}$ as a function of time,
471 from which recovery yields can be estimated.

472

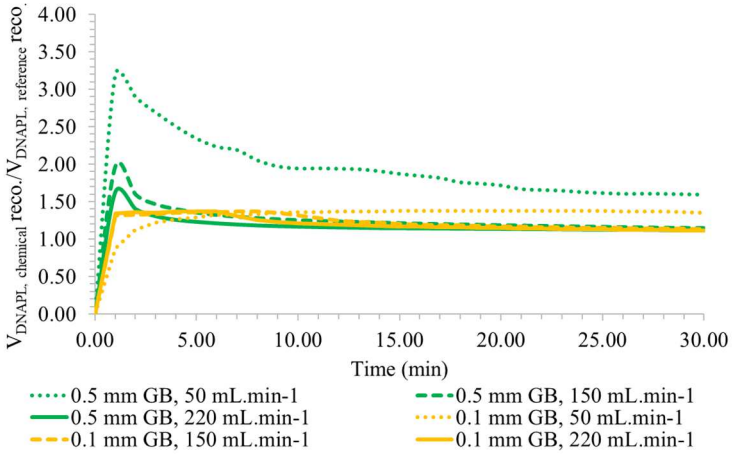

473

474 Figure 11: Modelled $V_{DNAPL, chemical}/V_{DNAPL, reference}$ recovered ratios as a function of time with 0.5 and

475 0.1 mm GB.

476

477 For the 0.1 mm GB, the $V_{DNAPL, chemical}/V_{DNAPL, reference}$ ratios were relatively stable over time and

478 were higher for lower flow rates (except for the very beginning of the experiment). Also, these ratios

479 were on average (between 5 min and 30 min) 1.37, 1.22, and 1.18 respectively for 50, 150, and 220

480 $mL.min^{-1}$. For the 0.5 mm GB, the ratios were much higher at the beginning of the experiment: ratios

481 observed at t=2 min were 2.90, 1.60, and 1.40 for 50, 150, and 220 $mL.min^{-1}$, respectively. For the rest

482 of the experiment, the ratios were lower. For example, values observed between times 5 min and 30

483 min, were on average 1.82, 1.21, and 1.14, for 50, 150, and 220 $mL.min^{-1}$, respectively. Results show

484 that the use of chemical enhancement was proportionally more advantageous for lower flow rates than

485 for higher flow rates. Figure 4A (Appendix) shows how S_w changed over time along the horizontal and

486 vertical profiles at the center of the 2D tank. The addition of surfactant makes it possible to increase

487 the cone of depression volumes and to decrease the residual saturation inside the cone of depression.

488 The average S_{rn} in the COD was about 0.09 for 0.5 mm GB and 0.08 for 0.1 mm GB. These S_{rn}

489 correspond to the results obtained during drainage-imbibition tests and are significantly smaller than

490 S_{rn} without enhancement.

491

4.3 Experiments in the 2D tank with thermal enhancement

Figure 12 shows measured and modelled volumes of DNAPL as a function of time (without enhancement as a reference and with thermal enhancement).

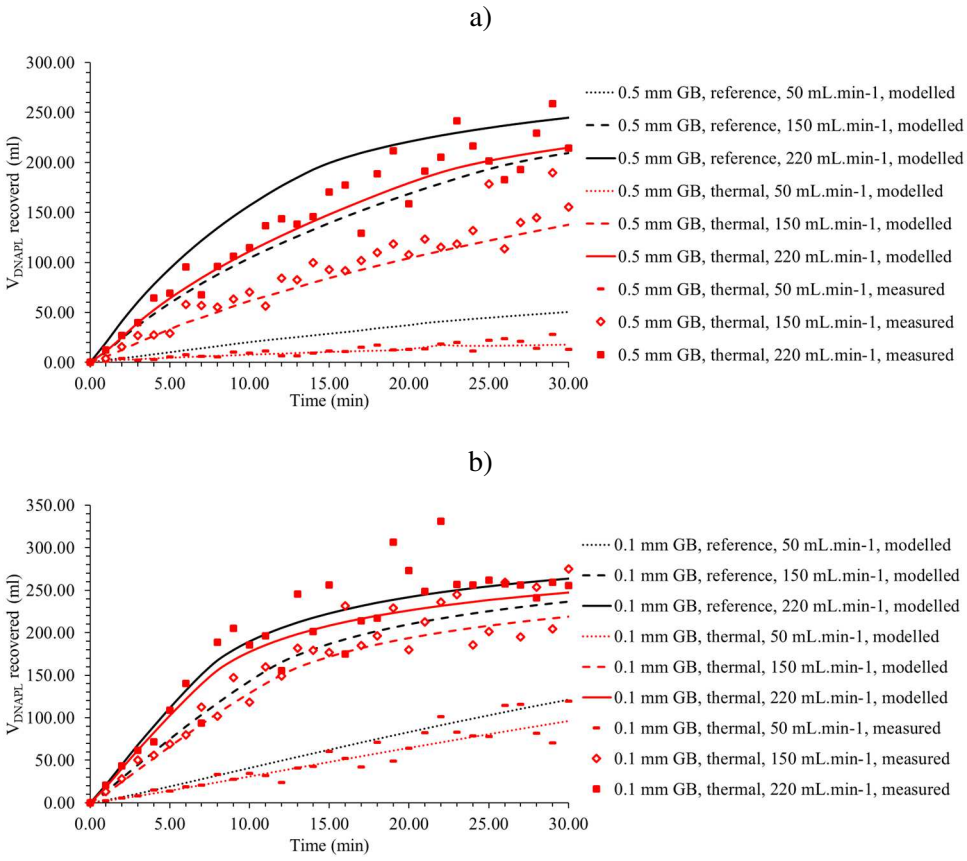

Figure 12: Evolution of measured (by image interpretation) and modelled volumes of DNAPL recovered for different flow rates with a) 0.5 mm GB and b) 0.1 mm GB (with thermal enhancement).

Results show that thermal enhancement did not have any beneficial effect on final recovery yield. The $V_{DNAPL\ recovered}$ with thermal enhancement represented on average 40, 60 and 76% of the $V_{DNAPL\ recovered}$ without enhancement for 0.5 mm GB (for 50, 150, and 220 mL.min^{-1}, respectively). For the 0.1 mm GB, these recovery yields were between 77, 91, and 93%. This was related to the reductions in fluid viscosity (μ_w/μ_n) and density (ρ_w/ρ_n) ratios, while the temperature increase was not sufficient to improve recovery rates and yields. Figure 5A (Appendix) compares the experimental results with the models and Figure 6A (Appendix) shows how S_w changed over time along the horizontal profile and

along a vertical profile at the center of the 2D tank. The decrease of DNAPL recovery volume with thermal enhancement is due to the fact that: i. the residual saturation in the cone of depression is identical to that of the reference (S_{rn}=0.10 and 0.14 for 0.5 and 0.1 mm GB, respectively) and, ii. the volume of this cone is smaller.

4.4 Comparison of fingering effects at the DNAPL-water interface without enhancement and with chemical and thermal enhancements

Figure 13 shows the flattened DNAPL-water interface for 0.5 and 0.1 mm GB at different flow rates (without enhancement).

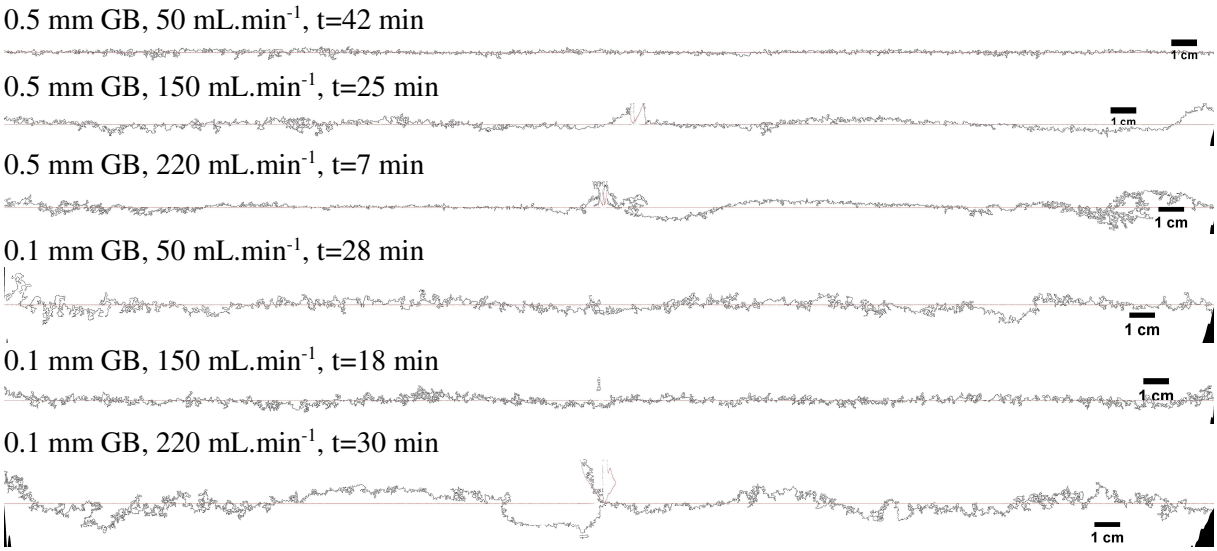

Figure 13: DNAPL-water interface flattened (without enhancement).

As stated above, the DNAPL-water interfaces were more tortuous for the 0.1 mm GB than for the 0.5 mm GB and the higher the flow rate, the more important was the fingering. Figure 14 shows the statistical representation of the fingerings of the DNAPL-water interfaces.

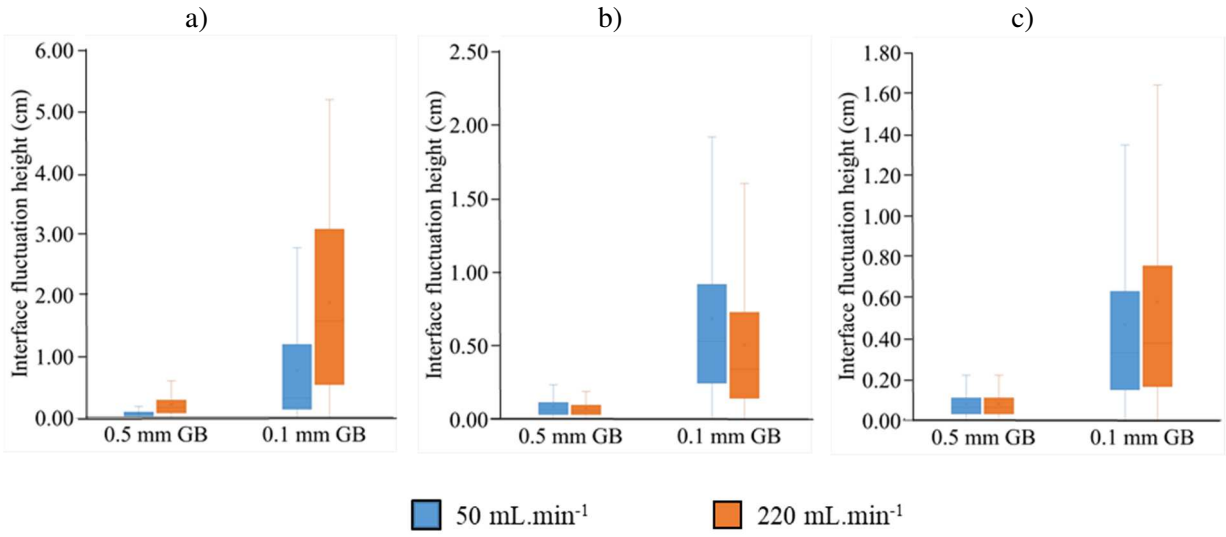

Figure 14: Statistical representation of fingerings of the DNAPL-water interface for 50 and 220 mL.min^{-1} with 0.5 and 0.1 mm GB (a) without enhancement, b) with chemical enhancement, and c) with thermal enhancement).

Regarding the experiments without enhancement, the DNAPL-water interface shapes were less irregular for the 0.5 mm GB than for the 0.1 mm GB. It highlights that fingering was more important for 0.1 mm GB than for 0.5 mm GB. The higher the pumping flow rate, the more fingering was observed. Regarding fingering without enhancement, the average value for 0.5 mm GB varied from 0.06 to 0.22 cm for flow rates from 50 to 220 mL.min^{-1} (with respective standard deviations of 0.05 to 0.21). The values were higher for the 0.1 mm GB: for flow rates of 50 to 220 mL.min^{-1}, the average values were respectively from 0.62 to 1.61 cm (with respective standard deviations of 0.42 and 1.14). Concerning the experiments with chemical enhancement, we observed that fingering was less important than for the experiments without enhancement. We noticed that, in this case, the fingering was also more important for the 0.1 mm GB than for the 0.5 mm GB: the average interface height fluctuations were respectively 0.54 and 0.07 cm (with average standard deviations of 0.44 and 0.07). Increasing the flow rate was found to have limited influence on fingering. Since the μ_w/μ_n ratios were lower, it explains why the fingerings were globally lower with thermal enhancement than without enhancement. The differences in fingering between the 0.5 and 0.1 mm GB were lower than for the reference case (without enhancement). The average interface heights were respectively 0.08 and 0.49 cm

for the 0.5 and 0.1 mm GB (with standard deviations of 0.07 and 0.40). The flow rate had little influence on fingerings; the differences in interface height between 50 and 220 mL.min^{-1} were 10 and 9% (respectively, for 0.5 and 0.1 mm GB).

Lenormand et al. (1988) have shown three multiphase domain displacements [Lenormand et al. (1988)]: i. Stable displacement where the main force is due to the viscosity of the injected fluid (capillary effects and pressure drop in the displaced fluid are negligible); ii. Viscous fingering where the main force is due to the viscosity of the displaced fluid (capillary effects and pressure drop in the displacing fluid are negligible); iii. Capillary fingering where at low N_{ca}, the viscous forces are negligible in both fluids and the main force is due to capillarity. Figure 15 shows our experimental results on the phase-diagram of multiphase domain displacement (capillary number as a function of the mobility ratios). The capillary number (N_{ca}) accounts for the ratio between viscous and capillary forces (Eq. 14) [Pennell et al. (1996)]. Shear forces, which depend on the viscosity contrast between wetting and non-wetting liquids, cannot be neglected for viscous liquids [Ng et al. (1978)]. In this case, the following mobility ratio can be used (m_r) (Eq. 15) [Dullien (1992)]:

$$N_{ca} = \frac{v_w \mu_w}{\sigma \cos\theta} \qquad \text{Eq. 14}$$

where v_w (m.s^{-1}) is the Darcy velocity of the wetting phase (upward direction is considered positive), μ_w (Pa.s) is the dynamic viscosity of the wetting phase, σ (mN.m^{-1}) is the interfacial tension, θ (°) is the DNAPL/water/glass contact angle.

$$m_r = \frac{k_{r,n} \mu_w}{k_{r,w} \mu_n} \qquad \text{Eq. 15}$$

where m_r (-) is the mobility ratio, $k_{r,w}$ (-) is the relative permeability for the displaced phase, $k_{r,n}$ (-) is the relative permeability for the displacing phase, μ_w (Pa.s) is the fluid dynamic viscosity for the displaced phase, and μ_n (Pa.s) is the fluid dynamic viscosity for the displacing phase.

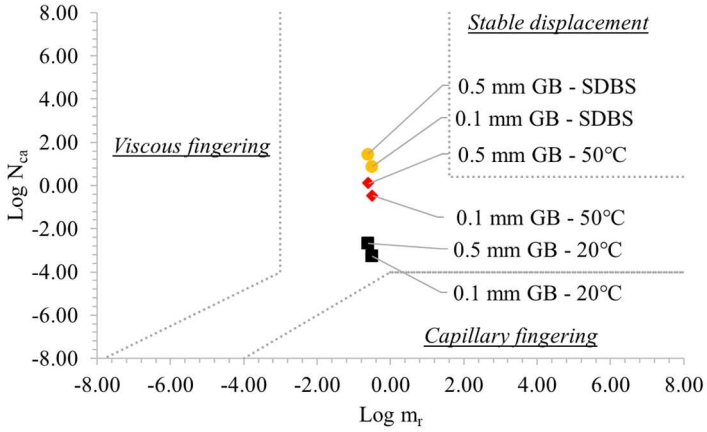

Figure 15: Representation of experimental results on the phase-diagram of multiphase domain displacement (adapted from [Lenormand et al. (1988)]).

Figure 15 highlights that fingerings were more important for 0.1 mm GB than for 0.5 mm GB. This was expected since the capillary effects are more important for 0.1 mm GB. Figure 15 shows also that the values for the 0.1 mm GB are always closer to the capillary fingering zone than the values for the 0.5 mm GB (N_{ca} are smaller). If we compare pumping without enhancement to pumping with enhancement, we note that for 0.5 and 0.1 mm GB, the values are much closer to the capillary fingering area. The thermal and chemical enhancement makes it possible to get closer to the stable displacement zone (by reducing the interfacial tensions and dynamic viscosities). These results agree with the experimental results relating to the measurements of DNAPL-water interface fluctuation heights.

5. Conclusions

The objectives of DNAPL pumping experiments in the 2D tank were: i. To verify that the proposed two-phase flow model was able to satisfactorily reproduce data measured during the experiments; ii. To compare the modelled water saturations to those derived from optical density measured over time during pumping tests performed at different flow rates; iii. To determine how chemical enhancement (addition of SDBS at its CMC to avoid DNAPL dissolution) and thermal enhancement (at 50°C to avoid DNAPL volatilization) affect DNAPL recovery yields and rates. The experiments were conducted with 0.5 and 0.1 mm GB.

585 Comparing experimental and modelled recovered DNAPL volumes shows that the model fits well
586 with the experiments and the image interpretation. Moreover, comparing experimental and modelled
587 values of radius and height of the cone of depression illustrates the validity of the model. The
588 numerical model was also able to successfully reproduce experimental results in the case of chemical
589 enhancement and thermal enhancement. The results showed that chemical enhancement has a
590 beneficial effect on recovered DNAPL volumes. The use of chemical enhancement was proportionally
591 more advantageous for lower flow rates than for higher flow rates. For the 0.1 mm GB the $V_{DNAPL,}$
592 $_{chemical}/V_{DNAPL,\ reference}$ ratios were relatively stable over time and were higher for lower flow rates than
593 for higher flow rates. The ratios were on average 1.37 and 1.18 for 50 and 220 $mL.min^{-1}$, resp. For the
594 0.5 mm GB, the ratios were much higher at the start of the experiment (the ratios were at 2 min, 2.90,
595 and 1.40 for 50 and
596 220 $mL.min^{-1}$, resp.). The cone of depression radius and height increased with the addition of
597 surfactant. Thermal enhancement (at 50°C) was not found to have any beneficial effect on DNAPL
598 recovery rate or yield. Heating the porous media had a negative effect on the cone of depression radius
599 and height.
600

601 **Acknowledgments**

602 This research was carried out as part of the SILPHES project supported by ADEME (French
603 Environment and Energy Management Agency) in the framework of the Future Investments
604 ("Investissements d'Avenir") funding scheme and the BRGM MULTISCALEXPER project. The
605 authors acknowledge ADEME and the BRGM/DEPA division for its financial support. The authors
606 also gratefully acknowledge the financial support provided to the PIVOTS project by the Centre – Val
607 de Loire region (ARD 2020 program and CPER 2015-2020) and the French Ministry of Higher
608 Education and Research (CPER 2015-2020 and public service subsidy to BRGM). Support from the
609 European Union via the European Regional Development Fund is also acknowledged. We thank
610 Stéphane Rivière, Yann Colombano and Stéphane Gaboreau for their advice on photographic
611 techniques, and INOVYN for the assistance provided during the SILPHES project, in particular for
612 providing access to the Tavaux site.

Appendix A

Figure 1A shows the results of a model parametric analysis.

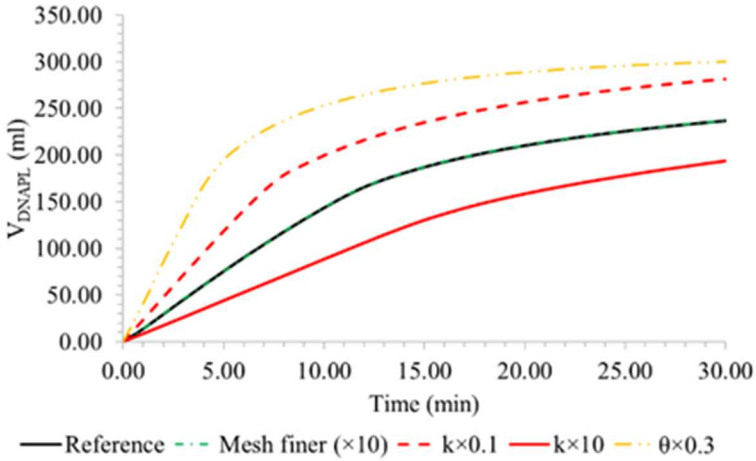

Figure 1A: Results of model parametric analysis (without enhancement).

A model parametric analysis (Figure 1A) was performed based on a reference experiment scenario (reference experiment: 0.1 mm GB, without enhancement, 150 mL.min^{-1}). Variations in the following parameters were considered: intrinsic permeability (k×0.1 and k×10), number of meshes (×10), porosity (θ×0.3).

Using a finer mesh (×10) did not influence the final result (+0.8%), which means that the number of meshes used in the model was sufficient.

The permeability variations (k×0.1 and k×10) reach respective differences for the volume of the DNAPL recovered at 30 min of +19% and -20% relative to the base scenario. The increase in these volumes with lower permeability (without changing curves $P_c=f(S_w)$) matches the differences observed between the 0.5 and 0.1 mm GB.

Decreasing the porosity (θ×0.3) increased the recovered volume of the DNAPL by 27% at 30 min.

Figure 2A shows the evolution of the modelled S_w along horizontal and vertical profiles at the center of the 2D tank without enhancement for different flow rates.

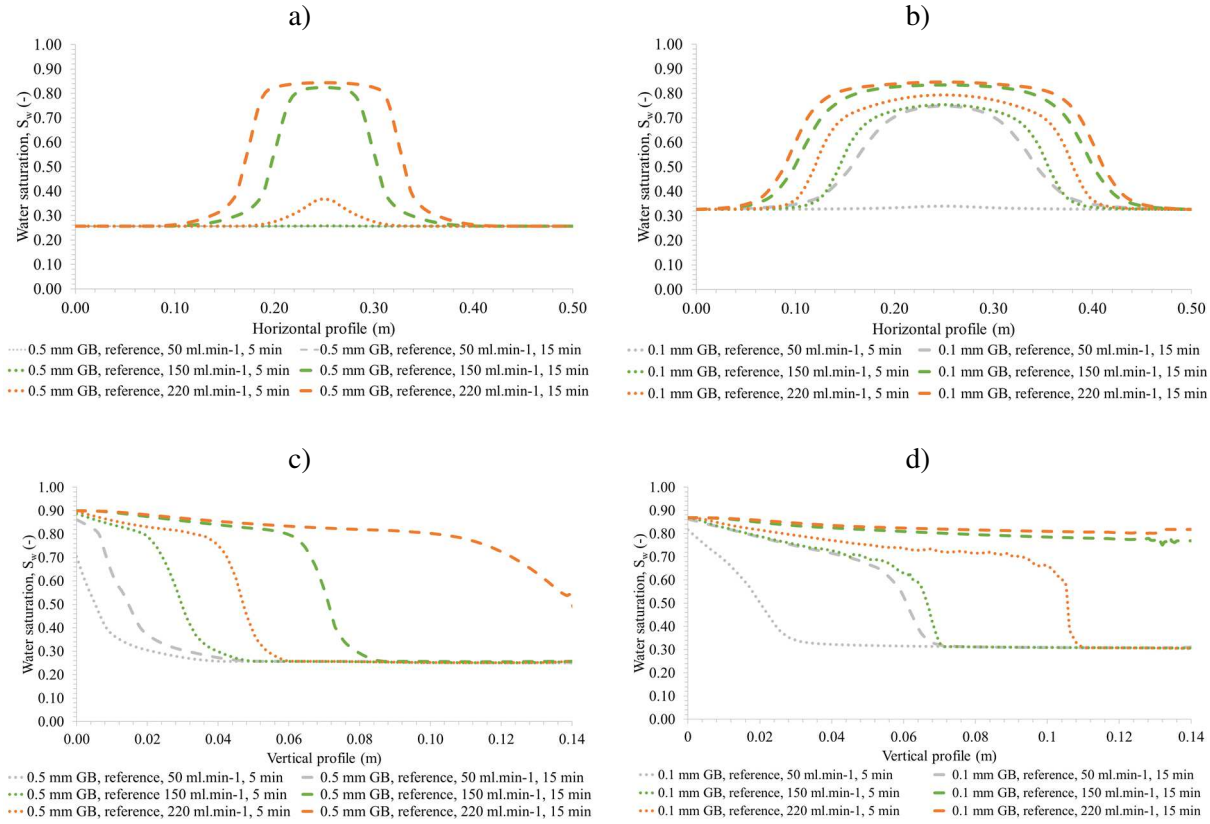

Figure 2A: Evolution of the modelled S_w along horizontal and vertical profiles at the center of the 2D tank without enhancement for 50, 150, and 220 mL.min^{-1} (horizontal profiles for a) 0.5 mm GB and b) 0.1 mm GB; vertical profiles for c) 0.5 mm GB and d) 0.1 mm GB).

The horizontal water saturation profile shows the cone of depression radii and capillary fringes (distance entre S_{rn} et S_{rw}). We see that the transition zones between S_{rn} and S_{rw} are sharper for the 0.5 mm GB than for the 0.1 mm GB. This can be explained by the fact that the capillary effect is more important for 0.1 mm GB than for 0.5 mm GB [Colombano et al. (2020)]. For example, this transition zone was 0.08 and 0.14 m at a flow rate of 150 mL.min^{-1} at t=15 min after the start of pumping, for

649 the 0.5 mm and 0.1 mm GB, respectively. Moreover, the radius of the cone of depression was higher
650 for the 0.1 mm GB than for the 0.5 mm GB. For example, it can be estimated (by measuring the length
651 of the curve's top plateau as a first approach) at 0.05 and 0.14 m for the 0.5 and 0.01 mm GB
652 respectively (for a flow rate of 150 $mL.min^{-1}$ at t=15 min after the start of pumping). From the vertical
653 saturation profile, we can also estimate the height of the cone of depression. For a flow rate of 150
654 $mL.min^{-1}$, the height at 5 min was 0.05 and 0.07 m for the 0.5 mm and 0.1 mm GB, respectively. The
655 graphs show a sharper capillary fringe for the 0.5 mm GB than the 0.1 mm GB. The DNAPL-water
656 transition zone was smaller when the flow rates were higher.
657
658

Figure 3A compares the experimental results with the model ones, for the chemical enhancement case.

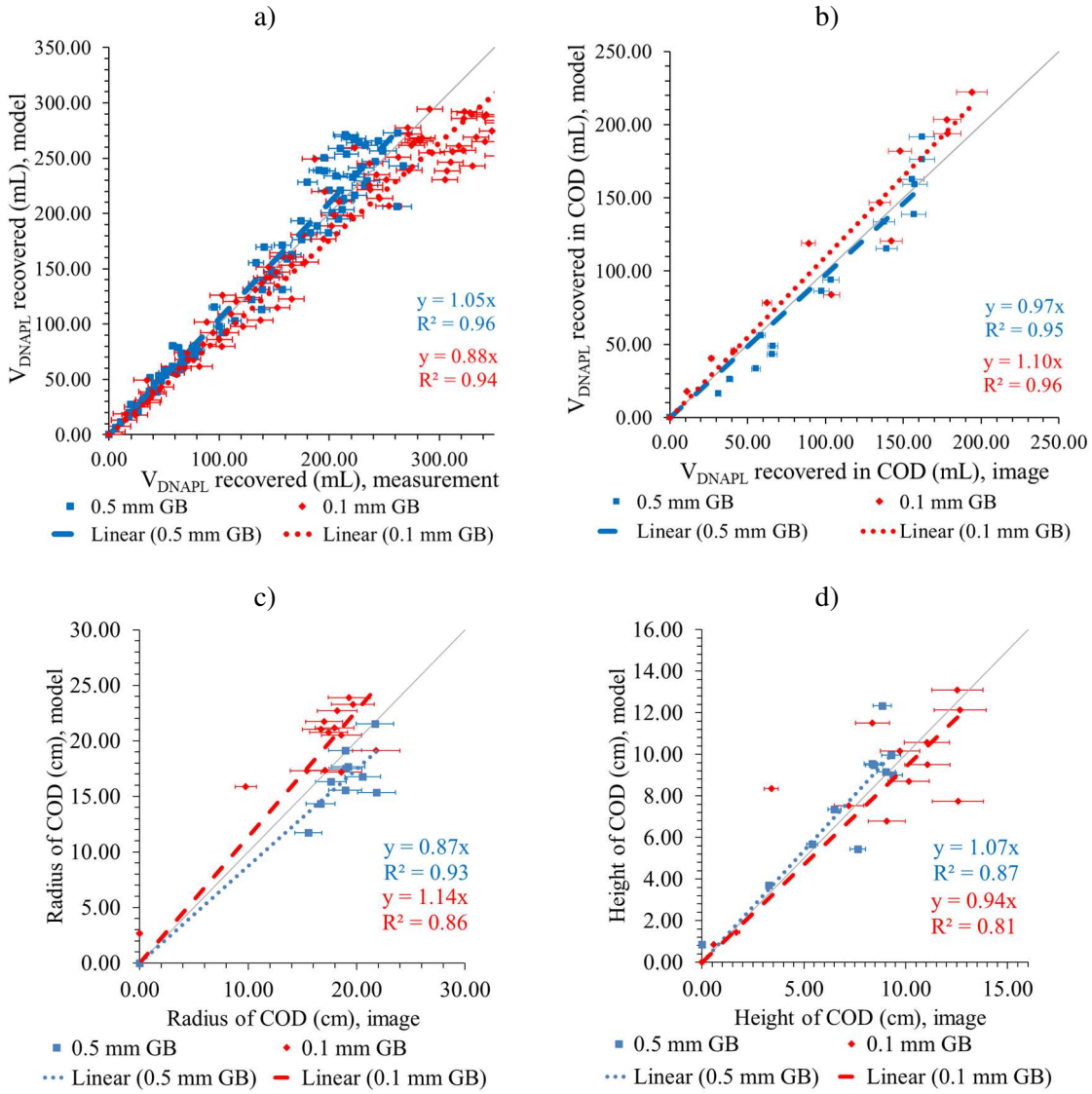

Figure 3A: Comparison of experimental and modelled results in the 2D tank with 0.5 and 0.1 mm GB (with chemical enhancement) for 150 mL.min^{-1}: a) volumes of recovered DNAPL estimated with image interpretation vs modelled volumes of DNAPL recovered, b) volumes of DNAPL recovered estimated with image interpretation vs modelled volumes of DNAPL estimated using the cone of depression zone, c) radius of the cone of depression estimated with image interpretation versus calculated with the model, and d) height of the cone of depression estimated with image interpretation versus calculated with the model.

The modelled $V_{DNAPL\ recovered}$ matched the measured $V_{DNAPL\ recovered}$ during the experiment. The slopes of $V_{DNAPL\ recovered\ modelled}=f(V_{DNAPL\ recovered\ measured})$ were close to 1 (1.05 and 0.88 respectively for 0.5 and 0.1 mm GB with R^2 of 0.96 and 0.94). The standard deviation was, as expected, lower for the 0.1 mm GB. The comparison of the estimated DNAPL volumes recovered experimentally (with image interpretation) with those calculated from modelling in the COD, shows that the modelling matched the image interpretations: the linear regression curve gradients were respectively 0.97 and 1.10 for the 0.5 and 0.1 mm GB. The R^2 values were acceptable (i.e., 0.95 and 0.96 for the 0.5 and 0.1 mm GB, resp.). As for the comparison of the measured and modelled radius and height of the cone of depression with 0.5 mm GB and 0.1 mm GB (Figure 3Ac and d), one can see that the linear regression $radius_{modelled}=f(radius_{measured})$ were 0.87 and 1.14, for 0.5 and 0.1 mm GB, resp. (with R^2 of 0.93 and 0.86). Moreover, the linear regression $height_{modelled}=f(height_{measured})$ were respectively 1.07 and 0.94 (with R^2=0.87 and 0.81). These regression coefficients highlight the satisfactory match between measured and modelled values. Compared to experiments without enhancement, the addition of surfactant makes it possible to increase the cone of depression volumes and to decrease the residual saturation inside the cone of depression.

Figure 4A shows how modelled S_w changed over time along the horizontal and vertical profiles at the center of the 2D tank with chemical enhancement for 150 mL.min^{-1}.

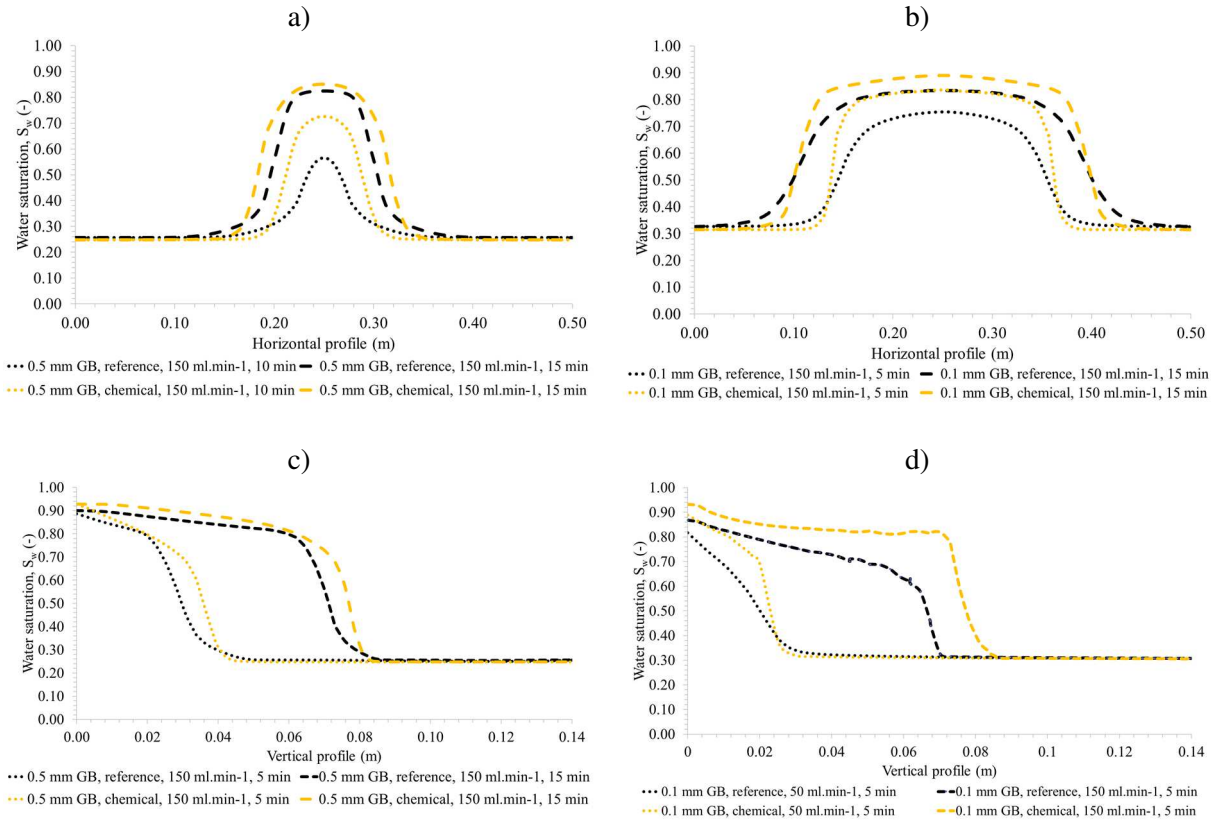

Figure 4A: Evolution of the modelled S_w along horizontal and vertical profiles at the center of the 2D tank with chemical enhancement for 150 mL.min^{-1} (horizontal profiles for a) 0.5 mm GB and b) 0.1 mm GB, vertical profiles for c) 0.5 mm GB and d) 0.1 mm GB).

The horizontal water saturation profile demonstrates the effectiveness of the chemical enhancement. For example, regarding 0.5 mm GB at 0.25 m, S_w was 0.72 at t=10 min with chemical enhancement but only 0.55 without enhancement. Regarding 0.1 mm GB, S_w was 0.83 at 0.25 m at t=5 min with chemical enhancement but only 0.75 without enhancement. The vertical water saturation profiles show that chemical enhancement increases the displacement of the two-phase front by more than 10% for the 0.5 mm GB and by 15% for the 0.1 mm GB (for S_w=0.6 for t=15 min).

Figure 5A compares the experimental results with the model ones in the 2D tank with 0.5 and 0.1 mm GB (with thermal enhancement) for 150 mL.min^{-1}.

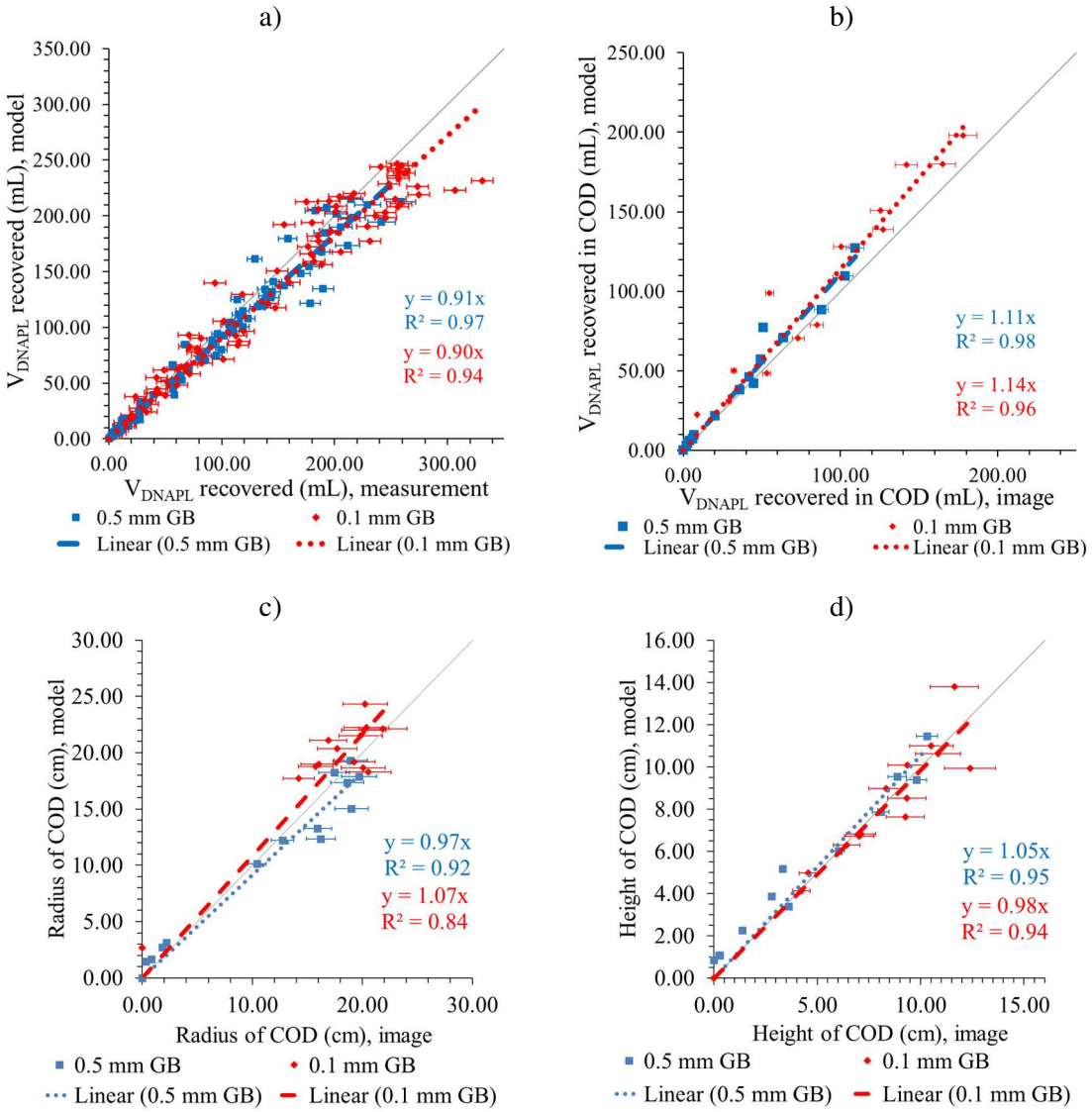

Figure 5A: Comparison of experimental and modelled results in the 2D tank with 0.5 and 0.1 mm GB (with thermal enhancement) for 150 mL.min^{-1}: a) volumes of recovered DNAPL estimated with image interpretation vs modelled volumes of DNAPL recovered, b) volumes of DNAPL recovered estimated with image interpretation vs modelled volumes of DNAPL estimated using the cone of depression zone, c) radius of the cone of depression estimated with image interpretation versus calculated with the model, and d) height of the cone of depression estimated with image interpretation versus calculated with the model.

714

715 The slopes of $V_{DNAPL\ recovered\ modelled}=f(V_{DNAPL\ recovered\ measured})$ were, as for the previous experiments
716 (without enhancement and with chemical enhancement), close to 1 (0.91 and 0.90 respectively for 0.5
717 and 0.1 mm GB with R^2 of 0.97 and 0.94). Again, as expected, the standard deviation was lower for
718 the 0.1 mm GB. Figure 5Ab compares estimated DNAPL volumes recovered experimentally (with
719 image interpretation) and by modelling (in the COD). The pumping experiments interpreted by image
720 analysis were well reproduced by the model. The linear regression curve gradients were respectively
721 1.11 and 1.14 for the 0.5 and 0.1 mm GB (with R^2 of 0.98 and 0.96). The comparison of experimental
722 and modelled radius and height of the cone of depression with 0.5 mm GB and 0.1 mm GB show
723 slopes of $radius_{modelled}=f(radius_{measured})$ close to 1: 0.97 and 1.07 for the 0.5 and 0.1 mm GB, resp. (with
724 R^2 of 0.92 and 0.84). Moreover, the slopes of $height_{modelled}=f(height_{measured})$ were respectively 1.05 and
725 0.98 (with R^2=0.95 and 0.94). The decrease in the recovery of DNAPL with thermal enhancement is
726 due to the fact that: i. the residual saturation in the cone of depression is identical to that of the
727 reference and, ii. the volume of this cone is smaller.
728

Figure 6A shows how modelled S_w changed over time along the horizontal profile and along a vertical profile at the center of the 2D tank with thermal enhancement for 150 mL.min^{-1}.

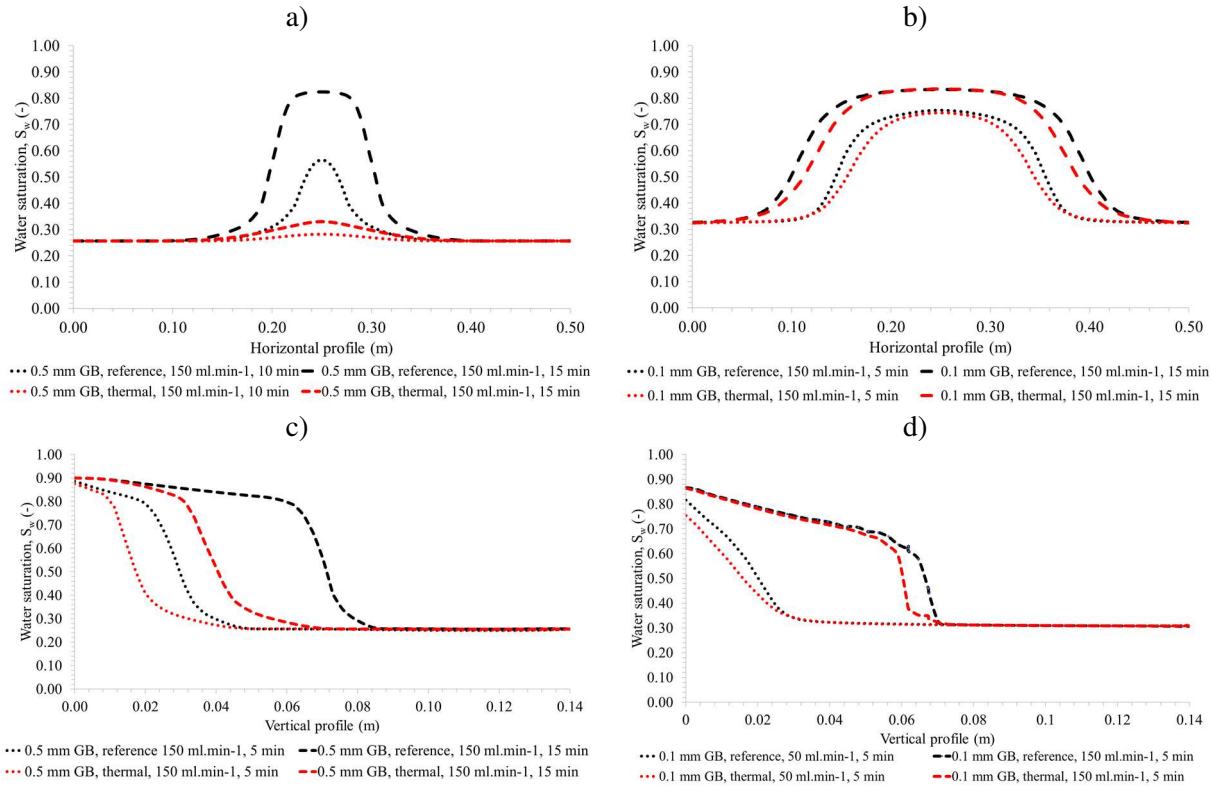

Figure 6A: Evolution of the modelled Sw along horizontal and vertical profiles at the center of the 2D tank with thermal enhancement for 150 mL.min^{-1} (horizontal profiles for a) 0.5 mm GB and b) 0.1 mm GB, vertical profiles for c) 0.5 mm GB and d) 0.1 mm GB).

The horizontal water saturation profile demonstrates that thermal enhancement was not effective. For example, for 0.5 mm GB at 0.25 m, S_w was 0.33 at t=10 min with thermal enhancement but 0.56 without enhancement. For the 0.1 mm GB, S_w at 0.17 m were 0.67 and 0.56 for experiments without and with thermal enhancement, resp., and at t=10 min. The vertical water saturation profile shows that thermal enhancement had a negative effect on the displacement of the migration front. We see that it reduced the displacement of the migration front by about 50% for the 0.5 mm GB and 20% for the 0.1 mm GB (for S_w=0.5 at t=15 min).

745 **References**

746 [Adamson and Gast (1997)] Adamson, A. and Gast, A.: 1997, *Physical Chemistry of Surfaces*,
747 number 0-471-14873-3, 5th edn, Wiley-Interscience, New York, NY, USA. 755 p.

748 [ADEME and Ernst & Young (2014)] ADEME and Ernst & Young: 2014, *Taux d'utilisation et coûts*
749 *des différentes techniques et filières de traitement des sols et des eaux souterraines polluées en France*
750 *– Synthèse des données 2012*, ADEME edn, Agence de l'Environnement et de la Maîtrise de
751 l'Energie, Agence de l'Environnement et de la Maîtrise de l'Energie - 20, avenue du Grésillé – BP
752 90406 – 49004 Angers Cedex 01. 148 p.

753 [Ahn et al. (2008)] Ahn, C., Kim, Y., Woo, S. and Park, J.: 2008, Soil washing using various
754 nonionic surfactants and their recovery by selective adsorption with activated carbon, *Journal of*
755 *Hazardous Materials* **154**(1–3), 153–160.

756 [Alazaiza et al. (2016)] Alazaiza, M., Nigien, S., Ishak, W. and Kamaruddin, S.: 2016, A review of
757 light reflection and transmission methods in monitoring non-aqueous phase liquid migration in porous
758 media, *Journal of Engeneering and Applied Sciences* **11**(4), 2319–2326.

759 [Alexandra et al. (2012)] Alexandra, R., Gerhard, J. and Kueper, B.: 2012, Hydraulic
760 Displacement of Dense Nonaqueous Phase Liquids for Source Zone Stabilization, *Groundwater*
761 **50**, 765–774.

762 [Antontsev (1972)] Antontsev, S.: 1972, On the solvability of boundary value problems for
763 degenerate two-phase porous flow equations, *Dinamika sploshnoy sredy* **10**, 28–53.

764 [Ataie-Ashtiani and Raeesi-Ardekani (2010)] Ataie-Ashtiani, B. and Raeesi-Ardekani, D.: 2010,
765 Comparison of Numerical Formulations for Two-phase Flow in Porous Media, *Geotechnical and*
766 *Geological Engineering* **28**(4), 373–389.

767 [Atteia et al. (2013)] Atteia, O., Del Campo Estrada, E. and Bertin, H.: 2013, Soil flushing: a
768 review of the origin of efficiency variability, *Reviews in Environmental Science and Bio/Technology*
769 **12**, 379–389.

770 [Banerjee (1984)] Banerjee, S.: 1984, Solubility of organic mixtures in water, *Environmental*
771 *Science & Technology* **18**(8), 587–591.

772 [Bastian (1999)] Bastian, P.: 1999, *Numerical Computation of Multiphase Flows in Porous*
773 *Media*, PhD thesis, Technischen Fakultät der Christian–Albrechts–Universität Kiel, Kiel, Germany.
774 222 p.
775 [Bear (1972)] Bear, J.: 1972, *Dynamics of Fluids in Porous Media*, number 9780486656755, Dover
776 Publications, New York, NY, USA. 800 p.
777 [Berglund and Cvetkovic (1995)] Berglund, S. and Cvetkovic, V.: 1995, Pump-and-Treat
778 Remediation of Heterogeneous Aquifers: Effects of Rate-Limited Mass Transfer, *Groundwater*
779 **33**, 675–685.
780 [Bjørnarå and Aker (2008)] Bjørnarå, T. and Aker, E.: 2008, Comparing Equations for Two-Phase
781 Fluid Flow in Porous Media, *COMSOL Conference 2008 Hannover*.
782 [Carey and McBean (2010a)] Carey, G. and McBean, E.: 2010a, A mass balance Approach for
783 estimating DNAPL Source remediation timeframe, *Proceedings of the 2010 RPIC Federal*
784 *Contaminated Sites National Workshop*, Montréal, Québec, Canada.
785 [Carey and McBean (2010b)] Carey, G. and McBean, E.: 2010b, Back-diffusion and discount rate
786 implications for DNAPL Remediation Strategies, *Proceedings of the 2010 RPIC Federal*
787 *Contaminated Sites National Workshop*, Montréal, Québec, Canada.
788 [Cary et al. (1989)] Cary, J., McBride, J. and Simmons, C.: 1989, Trichloroethylene residuals in
789 the capillary fringe as affected by air-entry pressure, *Journal of Environmental Quality* **18**, 72–77.
790 [Cazaux et al. (2014)] Cazaux, D., Colombano, S., Joubert, A., Dumestre, A. and Lecuelle, G.: 2014,
791 Optimized physical recovery of DNAPL using upwelling technique and geostatistical analysis at large
792 field scale, *Ninth International Conference on Remediation of Chlorinated and Recaclitrant*
793 *Compounds*, number A1, Battelle Press, Columbus, OH, USA, Monterey, CA, USA, p. 5.
794 [Chavent and Jaffre (1986)] Chavent, G. and Jaffre, J.: 1986, *Mathematical Models and Finite*
795 *Elements for Reservoir Simulation - Single Phase, Multiphase and Multicomponent Flows through*
796 *Porous Media*, Vol. 17, North-Holland, Amsterdam, Netherlands. 375 p.
797 [Chen and Ewing (1997)] Chen, Z. and Ewing, R.: 1997, Fully Discrete Finite Element Analysis
798 of Multiphase Flow in Groundwater Hydrology, *SIAM Journal on Numerical Analysis* **34**(6), 2228–
799 2253.

[Chen et al. (2006)] Chen, Z., Huan, G. and Ma, Y.: 2006, *Computational methods for multiphase flows in porous media*, number 978-0-898716-06-1, Philadelphia, PA , USA. 531 p.

[Childs et al. (2004)] Childs, J., Acosta, E., Knox, R., Harwell, J. and Sabatini, D.: 2004, Improving the extraction of tetrachloroethylene from soil columns using surfactant gradient systems, *Journal of Contaminant Hydrology* **71**(1-4), 27–45.

[Cohen and Mercer (1993)] Cohen, R. and Mercer, J.: 1993, DNAPL Site Evaluation, *Technical Report EPA/600/R-93/022*, Edited by USEPA Office of Research and Development. 369 p.

[Colombano et al. (2020)] Colombano, S., Davarzani, H., van Hullebusch, E., Huguenot, D., Guyonnet, D., Deparis, J. and Ignatiadis, I.: 2020, Thermal and chemical enhanced recovery of heavy chlorinated organic compounds in saturated porous media: 1D cell drainage-imbibition experiments, *Science of the Total Environment* **706**, 135758.

[Davarzani et al. (2014)] Davarzani, H., Smits, K., Tolene, R. and Illangasekare, T.: 2014, Study of the effect of wind speed on evaporation from soil through integrated modeling of the atmospheric boundary layer and shallow subsurface, *Water Resources Research* **50**(1), 661–680.

[Davis (1997)] Davis, E.: 1997, How Heat Can Enhance In-situ Soil and Aquifer Remediation:Important Chemical Properties and Guidance on Choosing the Appropriate Technique, *Technical Report EPA/540/S-97/502*, U.S. Environmental Protection Agency, U.S. Environmental Protection Agency; Solid Waste and Emergency Response, Washington, DC, USA. 18 p.

[Dullien (1992)] Dullien, F.: 1992, *Porous Media: Fluid Transport and Pore Structure*, number 978-0-12-223651-8, 2nd edn, Academic Press, San Diego, CA, USA. 574 p.

[Dwarakanath et al. (1999)] Dwarakanath, V., Kostarelos, K., Pope, G., Shotts, G. and Wade, W.: 1999, Anionic surfactant remediation of soil columns contaminated by nonaqueous phase liquids, *Journal of Contaminant Hydrology* **38**(4), 465–488.

[Esmaeili et al. (2019)] Esmaeili, S., Sarma, H., Harding, T. and Maini, B.: 2019, Review of the effect of temperature on oil-water relative permeability in porous rocks of oil reservoirs, *Fuel* **237**, 91–116.

[Falta et al. (2005b)] Falta, R., Basu, N. and Rao, P.: 2005b, Assessing impacts of partial mass depletion in DNAPL source zones: II. Coupling source strength functions to plume evolution, *Journal of Contaminant Hydrology* **79**(1-2), 45–66.

828 [Falta et al. (2005a)] Falta, R., Rao, P. and Basu, N.: 2005a, Assessing the impacts of partial mass
829 depletion in DNAPL source zones: I. Analytical modeling of source strength functions and plume
830 response, *Journal of Contaminant Hydrology* **78**(4.), 259–280.
831 [Feenstra et al. (1991)] Feenstra, S., Mackay, D. and Cherry, J.: 1991, A method for assessing residual
832 napl based on organic chemical concentrations in soil samples, *Groundwater Monitoring Review*
833 **11**(2), 128–136.
834 [Flores et al. (2011)] Flores, G., Katsumi, T., Inui, T. and Kamon, M.: 2011, A simplified image
835 analysis method to study LNAPL migration in porous media, soils and foundations, *Soils and*
836 *Foundations* **51**(5), 35–847.
837 [Fredenslund et al. (1975)] Fredenslund, A., Jones, R. and Prausnitz, J.: 1975, Group-contribution
838 estimation of activity coefficients in nonideal liquid mixtures, *American Institute of Chemical*
839 *Engineers Journal* **21**(6), 1086–1099.
840 [Grant and Gerhard (2007a)] Grant, G. and Gerhard, J.: 2007a, Simulating the dissolution of a
841 complex dense nonaqueous phase liquid source zone: 1. Model to predict interfacial area, *Water*
842 *Resources Research* **43**(W12410), 1–14.
843 [Grant and Gerhard (2007b)] Grant, G. and Gerhard, J.: 2007b, Simulating the dissolution of a
844 complex dense nonaqueous phase liquid source zone: 2. Experimental validation of an interfacial area-
845 based mass transfer model, *Water Resources Research* **43**(W12409), 1–18.
846 [Grant and Salehzadeh (1996)] Grant, S. and Salehzadeh, A.: 1996, Calculation of Temperature
847 Effects on Wetting Coefficients of Porous Solids and Their Capillary Pressure Functions, *Water*
848 *Resources Research* **32**(2), 261–270.
849 [Harendra and Vipulanandan (2011)] Harendra, S. and Vipulanandan, C.: 2011, Solubilization and
850 degradation of perchloroethylene (PCE) in cationic and nonionic surfactant solutions, *Journal of*
851 *Environmental Sciences* **23**(8), 1240–1248.
852 [Harkness and Konzuk (2014)] Harkness, M. and Konzuk, J.: 2014, *Cost analyses for remedial*
853 *options, in Chapter 16 in Chlorinated Solvent Source Zone Remediation*, number 978-1-4614-6921-6,
854 Springer, SERDP ESTCP Environmental Remediation Technology, New York, NY, USA. 713 p.

[Herbert et al. (2014)] Herbert, A., Carr, A. and Hoffmann, E.: 2014, Findfoci: A focus detection algorithm with automated parameter training that closely matches human assignments, reduces human inconsistencies and increases speed of analysis, *PLoS ONE* **9**(12), 1–33.

[Hopmans and Dane (1986)] Hopmans, J. and Dane, J.: 1986, Temperature dependence of soil water retention curves, *Soil Sci. Sac. Am. J.* **50**, 562–567.

[Huang et al. (2015)] Huang, J., Christ, J., Goltz, M. and Demond, A.: 2015, Modeling NAPL dissolution from pendular rings in idealized porous media, *Water Resources Research* **51**, 8182–8197.

[IARC (2018)] IARC: 2018. https://www.iarc.fr/

[Imhoff et al. (1993)] Imhoff, P., Jaffé, P. and Pinder, G.: 1993, An experimental study of complete dissolution of a nonaqueous phase liquid in saturated porous media, *Water Resources Research* **30**(2), 307–320.

[ITRC (2002)] ITRC: 2002, *DNAPL Source Reduction: Facing the Challenge*, Technical/Regulatory Guidelines, Interstate Technology & Regulatory Council, Washington, DC, USA. 40 p.

[ITRC (2015)] ITRC: 2015, *Integrated DNAPL Site Characterization and Tools Selection*, number ISC-1 in *Guidance Document*, Interstate Technology & Regulatory Council, Washington, DC, USA. 361 p.

[Kueper et al. (2003)] Kueper, B., Wealthall, G., Smith, J., Leharne, S. and Lerner, D.: 2003, *An illustrated handbook of DNAPL transport and fate in the subsurface*, number 1844320669, U.K. Environment Agency, Bristol, England, United Kingdom. 67 p.

[Lenormand et al. (1988)] Lenormand, R., Touboul, E. and Zarcone, C.: 1988, Numerical models and experiments on immiscible displacements in porous media, *Journal of Fluid Mechanics* **189**, 165–187.

[Lin et al. (1982)] Lin, C., Pinder, G. and Wood, E.: 1982, Water resources program report 83-wr-2.

[Luciano et al. (2018)] Luciano, A., Mancini, G., Torretta, V. and Viotti, P.: 2018, An empirical model for the evaluation of the dissolution rate from a DNAPL-contaminated area, *Environmental Science and Pollution Research* **25**, 3992–34004.

882 [Luciano et al. (2012)] Luciano, A., Viotti, P. and Papini, M.: 2012, On Morphometric Properties of
883 DNAPL Sources: Relating Architecture to Mass Reduction, *Water, Air, & Soil Pollution*
884 **223**(5), 2849–2864.
885 [Luciano et al. (2010)] Luciano, A., Viotti, P. and Papini, M. P.: 2010, Laboratory investigation of
886 DNAPL migration in porous media, *Journal of Hazardous Materials* **176**(1-3), 1006–1017.
887 [Mackay and Cherry (1989)] Mackay, D. and Cherry, J.: 1989, Groundwater contamination: pump-
888 and-treat remediation, *Environmental Science & Technology* **23**, 630–636.
889 [Mackay et al. (1985)] Mackay, D., Roberts, P. and Cherry, J.: 1985, Transport of organic
890 contaminants in groundwater, *Environmental Science & Technology* **19**(5), 384–392.
891 [Mackay et al. (1991)] Mackay, D., Shiu, W., Maijanen, A. and Feenstra, S.: 1991, Dissolution of
892 non-aqueous phase liquids in groundwater, *Journal of Contaminant Hydrology* **8**(1), 23–42.
893 [Maire et al. (2018)] Maire, J., Joubert, A., Kaifas, D., Invernizzi, T., Mardue, J., Colombano, S.,
894 Cazaux, D., Marion, C., Klein, P., Dumestre, A. and Fatin-Rouge, N.: 2018, Assessment of flushing
895 methods for the removal of heavy chlorinated compounds DNAPL in an alluvial aquifer, *Science of*
896 *the Total Environment* (612), 1149–1158.
897 [McDade et al. (2005)] McDade, J., McGuire, T. and Newell, C.: 2005, Analysis of DNAPL source-
898 depletion costs at 36 field sites, *Remediation Journal* **15**(2:), 9–18.
899 [McGuire et al. (2006)] McGuire, T., McDade, J. and Newell, C.: 2006, Performance of DNAPL
900 Source Depletion Technologies at 59 Chlorinated Solvent-Impacted Sites, *Ground Water Monitoring*
901 *and Remediation* **26**(1), 73–84.
902 [Miller et al. (1990)] Miller, C., Poirier-McNeill, M. and Mayer, A.: 1990, Dissolution of Trapped
903 Nonaqueous Phase Liquids: Mass Transfer Characteristics, *Water Resources Research* **26**(11), 2783–
904 2796.
905 [Mualem (1976)] Mualem, Y.: 1976, A new model for predicting the hydraulic conductivity of
906 unsaturated porous media, *Water Resources Research* **12**(3), 513–522.
907 [Nambi and Powers (2003)] Nambi, I. and Powers, S.: 2003, Mass transfer correlations for
908 nonaqueous phase liquid dissolution from regions with high initial saturations, *Water Resources*
909 *Research* **39**, 1030–1040.

910 [Newell and Adamson (2005)] Newell, C. and Adamson, D.: 2005, Planning-level source decay
911 models to evaluate impact of source depletion on remediation timeframe, *Remediation* **15**(4), 27–47.
912 [Ng et al. (1978)] Ng, K., Davis, H. and Scriven, L.: 1978, Visualization of blob mechanics in
913 flow through porous media, *Chemical Engineering Science* **33**(8), 1009–1017.
914 [NIEHS (2015)] NIEHS: 2015, Chlorinated organics – information page, website.
915 http://tools.niehs.nih.gov/srp/research/research4_s3_s4.cfm
916 [O'Carroll et al. (2004)] O'Carroll, D., Bradford, S. and Abriola, L.: 2004, Infiltration of PCE
917 in a system containing spatial wettability variations, *Journal of Contaminant Hydrology* **73**(1-4), 39–
918 63.
919 [Pankow and Cherry (1996)] Pankow, J. and Cherry, J.: 1996, *Dense Chlorinated Solvents and*
920 *Other DNAPLs in Groundwater: History, Behavior, and Remediation*, number 978-0964801417,
921 Waterloo Press, Portland, OR, USA. 525 p.
922 [Pennell et al. (2014)] Pennell, K., Capiro, N. and Walker, D.: 2014, *Surfactant and cosolvent*
923 *flushing, Chapter 11 in Chlorinated Solvent Source Zone Remediation*, number 978-1-4614-6921-6,
924 Springer, SERDP ESTCP Environmental Remediation Technology, New York, NY, USA. 713 p.
925 [Pennell et al. (1996)] Pennell, K., Pope, G. and Abriola, L.: 1996, Influence of viscous and
926 buoyancy forces on the mobilization of residual tetrachloroethylene during surfactant flushing,
927 *Environmental Science & Technology* **30**, 1328–1335.
928 [Philippe et al. (2020)] Philippe, N., Davarzani, H., Colombano, S., Dierick, M., Klein, P. and
929 Marcoux, M.: 2020, Experimental study of the temperature effect on two-phase flow properties in
930 highly permeable porous media: Application to the remediation of dense non-aqueous phase liquids
931 (DNAPLs) in polluted soil, *Advances in Water Resources* **146**(103783).
932 [Poston et al. (1970)] Poston, S., Ysrael, S., Hossain, A. and Montgomery III, E.: 1970, The Effect
933 of Temperature on Irreducible Water Saturation and Relative Permeability of Unconsolidated Sands,
934 *Society of Petroleum Engineers* **10**, 171–180.
935 [Poulsen and Kueper (1992)] Poulsen, M. and Kueper, B.: 1992, A field experiment to study the
936 behavior of tetrachloroethylene in unsaturated porous media, *Environmental Science and Technology*
937 **26**(5), 889–895.

938 [Rodrigues et al. (2017)] Rodrigues, R., Betelu, S., Colombano, S., Masselot, G., Tzedakis, T.
939 and Ignatiadis, I.: 2017, Influence of temperature and surfactants on the solubilization of
940 hexachlorobutadiene and hexachloroethane, *Journal of Chemical & Engineering Data* **62**(10), 3252–
941 3260.
942 [Rosen (1989)] Rosen, M.: 1989, *Surfactants and Interfacial Phenomena*, 2nd edn, John Wiley and
943 Sons, New York, NY, USA. 431 p.
944 [Rueden et al. (2017)] Rueden, C., Schindelin, J., Hiner, M., DeZonia, B., Walter, A., Arena, E. and
945 Eliceiri, K.: 2017, Imagej2: Imagej for the next generation of scientific image data, *BMC*
946 *Bioinformatics* **18**(529), 1–26.
947 [Sabatini et al. (1998)] Sabatini, D., Harwell, J., Hasegawa, M. and Knox, R.: 1998, Membrane
948 processes and surfactant-enhanced subsurface remediation: results of a field demonstration, *Journal of*
949 *Membrane Science* **151**(1), 87–98.
950 [Sabatini et al. (2000)] Sabatini, D., Knox, R., Harwell, J. and Wu, B.: 2000, Integrated design of
951 surfactant enhanced DNAPL remediation: Efficient supersolubilization and gradient systems, *Journal*
952 *of Contaminant Hydrology* **45**(1-2), 99–121.
953 [Sale (2001)] Sale, T.: 2001, Methods for Determining Inputs to Environmental Petroleum
954 Hydrocarbon Mobility and Recovery Models, *Technical Report API PUBLICATION 4711*, American
955 Petroleum Institute, 1220 L Street, Northwest., Washington, DC, USA. 72 p.
956 [Schincariol et al. (1993)] Schincariol, R., Herderick, E. and Schwartz, F.: 1993, On the
957 application of image analysis to determine concentration distributions in laboratory experiments,
958 *Journal of Contaminant Hydrology* **12**(3), 197–215.
959 [Schindelin et al. (2012)] Schindelin, J., Arganda-Carreras, I., Frise, E., Kaynig, V., Longair,
960 M., Pietzsch, T., Preibisch, S., Rueden, C., Saalfeld, S., Schmid, B., Tinevez, J.-Y., White, D.,
961 Hartenstein, V., Eliceiri, K., Tomancak, P. and Cardona, A.: 2012, Fiji: an open-source platform for
962 biological-image analysis, *Nature methods* **9**(7), 676–682.
963 [Schlüter (2008)] Schlüter, M.: 2008, Geometric mappings.
964 http://ij.ms3d.de/geometric_mappings.php

965 [Schwille (1988)] Schwille, F.: 1988, *Dense Chlorinated Solvents in Porous and Fractured*
966 *Media - Model Experiments*, number 978-0873711210, Lewis Publishers, Chelsea, MI, USA. 146 p.
967 [She and Sleep (1998)] She, H. and Sleep, B.: 1998, The effect of temperature on capillary pressure-
968 saturation relationships for air-water and perchloroethylene-water systems, *Water Resources Research*
969 **34**(10), 2587–2597.
970 [Sinnokrot et al. (1971)] Sinnokrot, A., Ramey, H. and Marsden, S.: 1971, Effect of
971 Temperature Level upon Capillary Pressure Curves, *Society of Petroleum Engineers* **11**, 13–22.
972 [Sleep and Ma (1997)] Sleep, B. and Ma, Y.: 1997, Thermal variation of organic fluid properties and
973 impact on thermal remediation feasibility, *Journal of Soil Contamination* **6**(3), 281–306.
974 [Stimson (1974)] Stimson, A.: 1974, *Photometry and Radiometry for Engineers*, number 978-
975 0471825319, John Wiley & Sons Inc, New York, NY, USA. 488 p.
976 [Stroo et al. (2012)] Stroo, H., Leeson, A., Marqusee, J., Johnson, P., Ward, C., Kavanaugh, M.,
977 Sale, T., Newell, C., Pennell, K., Lebrón, C. and Unger, M.: 2012, Chlorinated ethene source
978 remediation: lessons learned, *Environmental Science & Technology* **46**(6438–6447).
979 [Stroo et al. (2003)] Stroo, H., Unger, M., Ward, C., Kavanaugh, M., Vogel, C., Leeson, A.,
980 Marqusee, J. and Smith, B.: 2003, Peer Reviewed: Remediating Chlorinated Solvent Source Zones, A
981 workshop lists the challenges and research needs, *Environmental Science & Technology*
982 **37**(11), 224A–230A.
983 [Stupp and Paus (1999)] Stupp, H. and Paus, L.: 1999, Migrationsverhalten organischer
984 Grundwasser-Inhaltsstoffe und daraus resultierende Ansätze zur Beurteilung von Monitored Natural
985 Attenuation (MNA), *TerraTech* (5).
986 [Suchomel et al. (2007)] Suchomel, E., Ramsburg, C. and Pennell, K.: 2007, Evaluation of
987 trichloroethene recovery processes in heterogeneous aquifer cells flushed with biodegradable
988 surfactants, *Journal of Contaminant Hydrology* **94**(3-4), 195–214.
989 [Taylor et al. (2001)] Taylor, T., Pennell, K., Abriola, L. and Dane, J.: 2001, Surfactant enhanced
990 recovery of tetrachloroethylene from a porous medium containing low permeability lenses: 1.
991 Experimental studies, *Journal of Contaminant Hydrology* **48**(3–4), 325–350.

992 [Travis and Doty (1990)] Travis, C. and Doty, C.: 1990, Can contaminated aquifers at
993 Superfund sites be remediated?, *Environmental Science & Technology* **24**, 1464–1466.
994 [Tseng (2011)] Tseng, Q.: 2011, *Etude d'architecture multicellulaire avec le microenvironnement*
995 *contrôlé*, PhD thesis, Université de Grenoble, France. 214 p.
996 [van Genuchten (1980)] van Genuchten, M.: 1980, A closed-form equation for predicting the hydraulic
997 conductivity of unsaturated soils, *Soil Science Society of America* **44**, 892–898.
998 [Wang and Beckermann (1993)] Wang, C.-Y. and Beckermann, C.: 1993, A two-phase mixture
999 model of liquid-gas flow and heat transfer in capillary porous media—I. Formulation, *International*
1000 *Journal of Heat and Mass Transfer* **36**(11), 2747–2758.
1001 [Zhao et al. (2006)] Zhao, B., Zhu, L. and Yang, K.: 2006, Solubilization of DNAPLs by mixed
1002 surfactant: Reduction in partitioning losses of nonionic surfactant, *Chemosphere* **62**(5), 772–779.
1003 [Zhong et al. (2003)] Zhong, L., Mayer, A. and Pope, G.: 2003, The effects of surfactant
1004 formulation on nonequilibrium NAPL solubilization, *Journal of Contaminant Hydrology* **60**(1-2), 55–
1005 75.
1006

Graphical abstract